EGG-2702

Review of Nonconventional Bioreactor Technology

C. E. Turick
M. E. McIlwain

Published September 1993

Idaho National Engineering Laboratory
EG&G Idaho, Inc.
Idaho Falls, Idaho 83415

Prepared for the
U.S. Department of Energy
Under DOE Idaho Operations Office
Contract DE-AC07-76ID01570

ABSTRACT

Biotechnology will significantly affect many industrial sectors in the future. Industrial sectors that will be affected include pharmaceutical, chemical, fuel, agricultural, and environmental remediation. Future research is needed to improve bioprocessing efficiency and cost-effectiveness in order to compete with traditional technologies. This report describes recent advances in bioprocess technologies and bioreactor designs and relates them to problems encountered in many industrial bioprocessing operations. The primary focus is directed towards increasing gas and vapor transfer for enhanced bioprocess kinetics as well as improved by-product separation and removal. The advantages and disadvantages of various conceptual designs such as hollow-fiber, gas-phase, hyperbaric/hypobaric, and electrochemical bioreactors are also discussed. Specific applications that are intended for improved bioprocesses include coal desulfurization, coal liquefaction, soil bioremediation, biomass conversion to marketable chemicals, biomining, and biohydrometallurgy as well as bioprocessing of gases and vapors.

CONTENTS

FIGURES

TABLES

REVIEW OF NONCONVENTIONAL BIOREACTOR TECHNOLOGY

Advances in biotechnology within the past decade have placed this field at the center of attention from both an economic and scientific perspective. Biotechnology has significant potential to positively affect numerous industrial sectors, including:

- Pharmaceutical
- Chemical
- Fuel
- Agricultural
- Environmental remediation
- Pollution control technologies.

The economic feasibility of many biotechnologies is largely dependent on efficient and cost-effective bioprocesses. To surpass or at least compete with traditional technologies, many bioprocesses will need to demonstrate consistent and practical operations.

The purpose of this review is to present information concerning recent advances in bioprocess technologies and relate them to current problems encountered in many industrial bioprocessing endeavors. Areas of interest that pertain to this review are high solids bioprocessing such as:

- Coal desulfurization
- Coal liquefaction
- Contaminated soil bioremediation
- Biomass conversion to marketable chemicals
- Biomining
- Biohydrometallurgy.

Another aspect of biotechnology of interest is that of bioprocessing of gases and vapors. Specific examples include synthesis and combustion gases such as volatile organic carbon (VOC), CO, CH_4, CO_2, H_2, and NO_X. Since VOC is a very broad term, this particular group of chemicals is also associated with environmental contamination by gasoline, diesel fuel, and chlorinated hydrocarbons.

Problems encountered in bioprocessing of the above mentioned substrates include:

- Increasing mass transfer of gaseous compounds introduced into a bioreactor
- Minimizing imbalanced conditions
- Product separation
- Maintaining the desired population of cells within the bioreactor
- Optimizing light penetration for photosynthetic organisms.

This review will address each of these topics and more recent technological advances that attempt to solve common problems of industrial bioprocessing and bioreactor design.

GAS-LIQUID MASS TRANSFER IN BIOREACTORS

Bioprocesses involving the use of gases must be designed to optimize the mass transfer of the gas or gases from the gas phase to the liquid phase via the gas-liquid interface and allow the gas to diffuse through the culture medium and to the cell surface where transport into the cell takes place. Because of the low solubility of many gases used in biotechnology, gas mass transfer is often the rate limiting step. The primary resistance to gas mass transfer may be assumed to be in the liquid film at the gas-liquid interface for sparingly soluble gases and can be described by the equation:

$$moles\ transported = \frac{K_L a}{H\ (P^G - P^L)} \quad (1)$$

where

$K_L a$ = overall gas mass transfer coefficient

H = Henry's law constant

P^G = substrate partial pressure in gas phase

P^L = substrate partial pressure at equilibrium with the substrate concentration in the bulk liquid phase.

Cells in the liquid phase consume the substrate at a maximum rate of:

$$moles\ consumed = qXV_L \quad (2)$$

where

q = specific uptake rate

X = cell density

V_L = liquid volume.

A microbial culture growing in liquid medium not limited by gas mass transfer will be limited by microbial kinetics. Important design characteristics for a bioreactor include specific interfacial area, liquid retention, and mass transfer coefficients. Conventional bioreactors in common use are mechanically stirred tank bioreactors, bubble columns, and packed bed columns. Aerobic bioprocesses requiring oxygen as the only gas can be designed to be either batch or continuous operations. Bioreactors for the use of synthesis gas or combustion gases need to be continuous operations because of the large volume of gases encountered.[1]

Continuous systems that have demonstrated high mass transfer rates include constantly stirred tank reactors (CSTR), immobilized cell bioreactors (ICBs), and trickle bed bioreactors. CSTRs have been shown to have an 80% efficiency rate of synthesis gas conversion.[2] Slightly soluble gases need rapid stirring rates in these bioreactors, which increases the operational costs. Assuming a CSTR has a low hydraulic and solids retention time, high microbial biomass can be achieved and maintained. This is necessary to maximize gas conversion kinetics and decrease gas retention time in the bioreactor. Since the bioreactor size is a direct function of microbial reaction rate and gas retention time, a CSTR has a volume limitation because of heating costs.

Immobilized cell bioreactors (ICBs) allow for high cell density and plug flow operation, which allows for high surface to volume ratios and high mass transfer rates. Klasson et al.[2] have demonstrated higher efficiency of gas conversion with immobilized cell bioreactors than CSTRs. Because of the high cell density and no stirring requirements of ICBs, they are potentially more economically feasible to operate.

Trickle bed columns allow gas in the continuous phase to pass over microbial cells growing on a fixed surface with nutrients passing over the surface. In order to increase reaction rates in these bioreactors, the solid supports can be configured to increase surface area and allow for higher cell density. Nutrient flow can be either concurrent or countercurrent to the flow of gas.

Several nonconventional technologies have been employed recently to deal with gas mass

transfer in bioreactors. Brauer[3] and Brauer and Annachhatre[4] demonstrated the application of the reciprocating jet bioreactor in increasing mass transfer of oxygen to bacterial and fungal cultures. The design of this bioreactor system consists of two units with a reciprocating jet bioreactor (HR), which is a cylindrical glass vessel (GZ) (diameter/height ratio either 1:2 or 1:4), located in the heart of each unit (see Figure 1). The volume of the bioreactors is either 12.5 dm^3 or 20 dm^3. HS is the reciprocating axis of HR, on which a package of sieve plates (LS) is mounted. The reciprocating motion of this system is achieved by the electronic motor (M) and a special crank gear (KT). The reciprocating motion of this system can vary from 0.25–1.25 Hz, while the amplitude remains constant at 100 mm (the optimum value).

The sieve plates are 50 mm apart, making the ratio of amplitude of the reciprocating motion and distance between plates 2. The diameter of the holes in the sieve plates is 12 mm, spaced 27 mm apart and arranged in the corners of a triangulum, with 11% making up the free area of the holes of the plate. Top and bottom lids (DP and BP) are stainless steel. DP contains openings for the reciprocating axis HS, for exit air (LA), substrate (SZ), inoculum (IZ), antifoam agent (AS), and for various instruments. Openings in the bottom lid are for air introduction (LZ), and biosuspension sampling (FP).

The bioreactor operates in a vertical reciprocating manner to allow fluid to flow through the holes in the plates, thus increasing turbulence and mixing of the cells, nutrients, and gases within the plates as well as among the plates. Both reciprocating jet bioreactors are operated independently of each other in alternating vertical motion, thereby maintaining the same total volume throughout the two systems (see Figure 2).

Oxygen transfer in the reciprocating jet bioreactor has been reported to be very efficient[3,5] and can be correlated by the following equation:

$$\frac{M_{o,max}}{V} = c(N/V)^{1/2} \qquad (3)$$

where

$M_{o,max}$ = oxygen transfer rate for maximum gas flow rate (flow rate just before dispersion of the air breaks down and flooding of the package plates begins)

V = bioreactor volume

N = input of mechanical energy per unit of time.

The empirical constant c = 2.05 for this bioreactor. The values for c for turbine stirrers and bubble columns are 1.45 and 0.69 respectively, thereby demonstrating superior operation efficiency with a reciprocating jet bioreactor.

The equation above can be applied in the range

$$1 < \frac{M_{o,max}}{N} < 6 \quad . \qquad (4)$$

Since N is proportional to the third power of the frequency f, the oxygen transfer rate is given by the proportionality:

$$M_{o,max} \text{ is proportional to } f^{3/2} \quad . \qquad (5)$$

Oxygen transfer increases with frequency but the energy requirement increases even more so.

Another way to express the rate of oxygen transfer is with the equation:

$$M_{o,max} = \beta a_p \Delta Po \qquad (6)$$

where

ß = time mean value of the mass transfer coefficient taken over time of half a cycle

a_p = specific interfacial area

ΔPo = mean difference of oxygen concentration in the bulk of the fluid and in the interface of the bubble

βa_p = proportional to $f^{3/2}$.

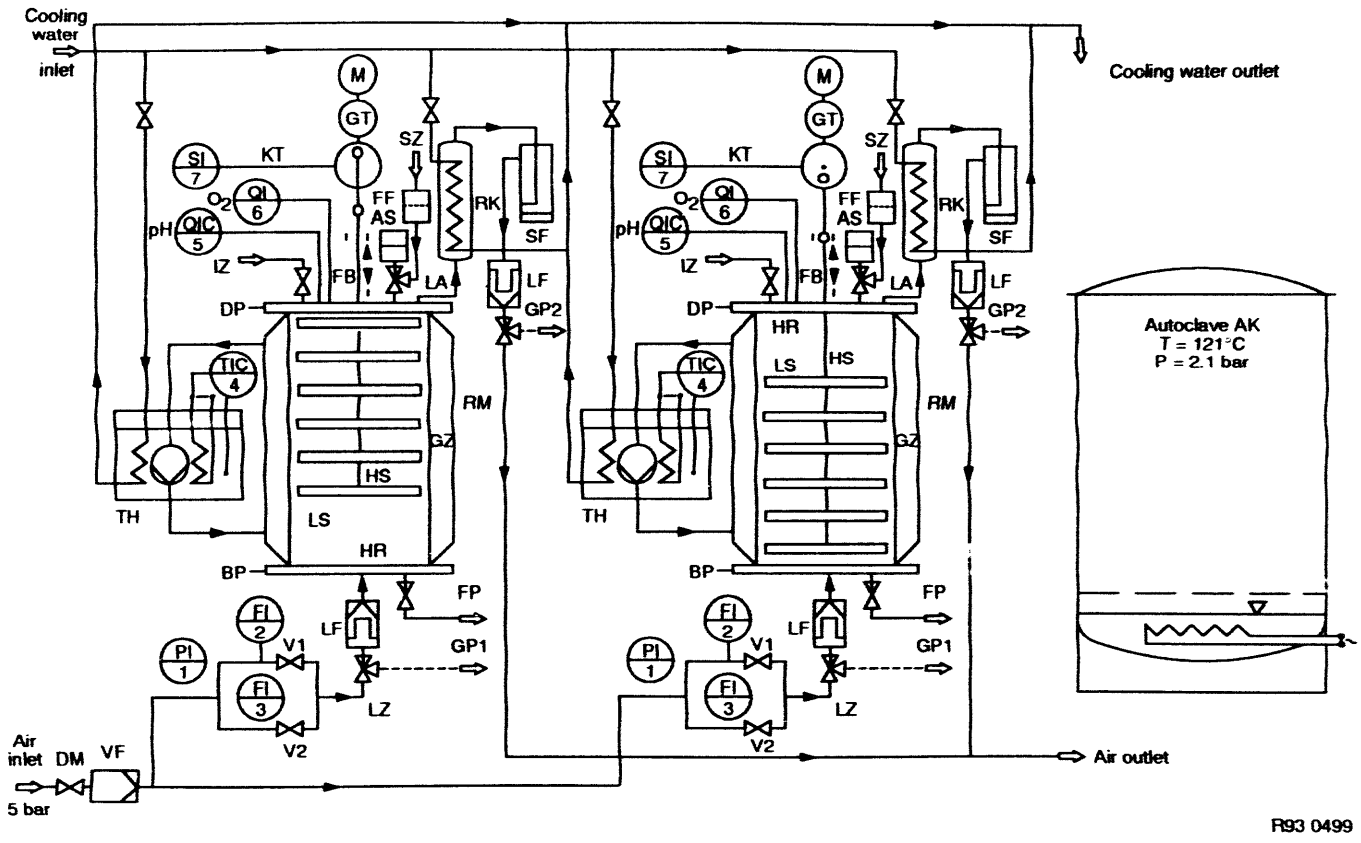

Figure 1. Schematic drawing of the experimental facility consisting of two identical units.

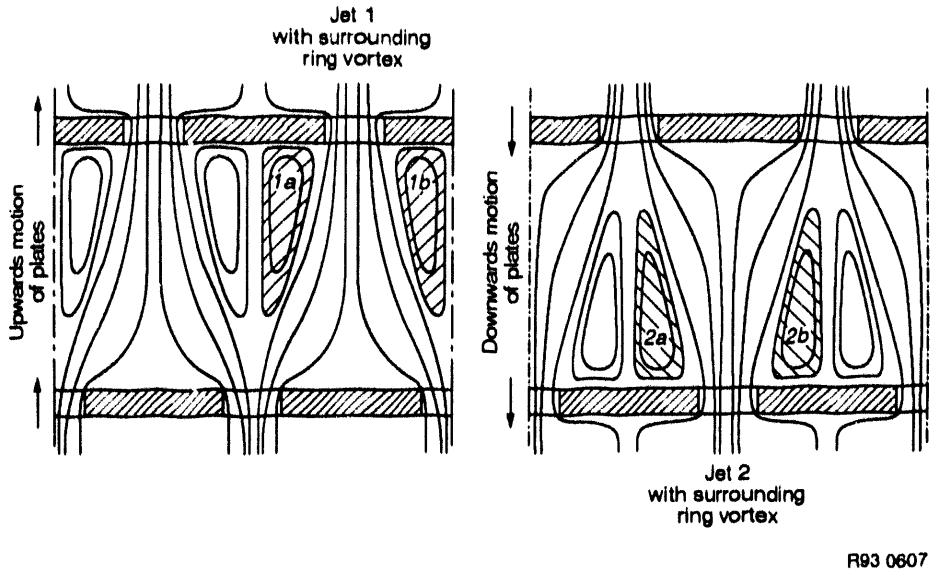

Figure 2. Schematic drawing for illustration of fluid motion in a volumetric element of the bioreactor.

Although faster agitation and stirring facilitate greater mixing and gas mass transfer, the costs involved can be prohibitive. Shear forces from violent mixing have been shown to damage cells and can also disrupt gel beads containing immobilized cells. Several methods have been developed to facilitate gas mass transfer while avoiding violent agitation. Shi et al.[6] reported a new impeller design for mammalian cell culture using an annular cage impeller with an increased surface area that increases convective oxygen transfer and reduces hydrodynamic shear damage to the cells. This design increased the oxygen transfer rate, cell density, and product concentration in batch cultures. In this design, oxygen is transferred from an air bubble rising in the liquid medium where oxygen transfer occurs at the air-liquid interface and bulk flow across the wire screen of the annular cage impeller. The oxygenated medium is then transported through the screen. The following equation gives the relationship between overall oxygen transfer resistance and the oxygen transfer resistances in the air-liquid region and the liquid-wire screen region:

$$\frac{1}{[V_l((k_La)_T - (k_La)_A)]} = \frac{1}{[V_c(k_La)_B]} + \frac{1}{[(V_l - V_c)(K_La)_S]} \quad (7)$$

where

$(k_La)_T$ = overall volumetric oxygen transfer coefficient

$(k_La)_A$ = volumetric oxygen transfer coefficient for surface aeration

$(k_La)_B$ = air-liquid volumetric oxygen coefficient inside the cage

$(k_La)_S$ = liquid-wire screen volumetric oxygen transfer coefficient

V_l and V_c = bioreactor working volume and the volume of the cage.

Figure 3 shows the improved monoclonal antibodies (MAb) production with this new impeller design with increased oxygen transfer rates.

Reiter et al.[7] developed a method to allow for rapid mixing within the bioreactor for increased oxygen solubility where oxygen is dissolved in a liquid medium before contacting cells in microcarriers grown in a caged, vibrating growth chamber (see Figures 4 and 5). In this way immobilized cells are not damaged by hydrodynamic shear forces. The cage is vibrated at a minimum amplitude (<0.3 mm) and frequency (50 Hz) to prevent

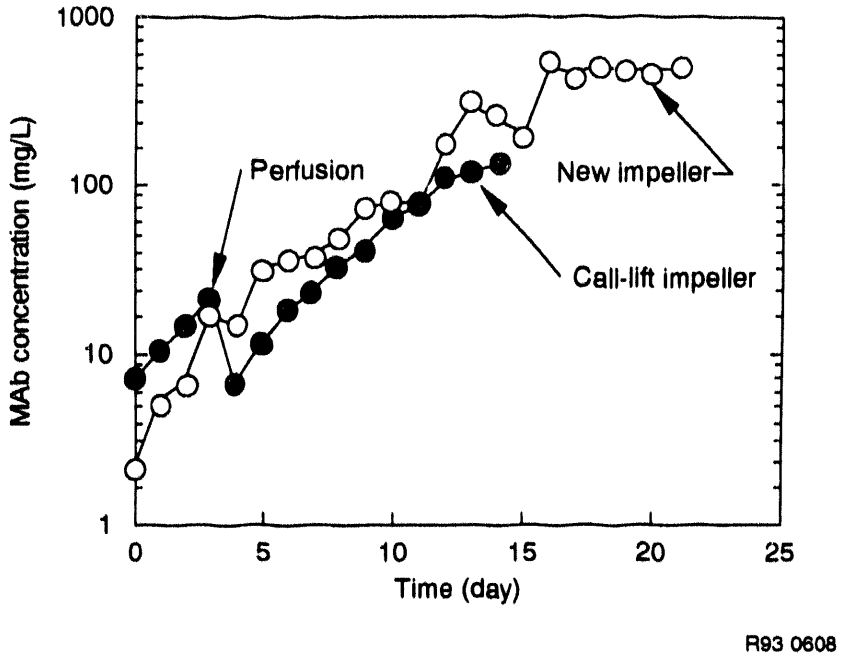

Figure 3. Time course of MAb production with two impeller designs.

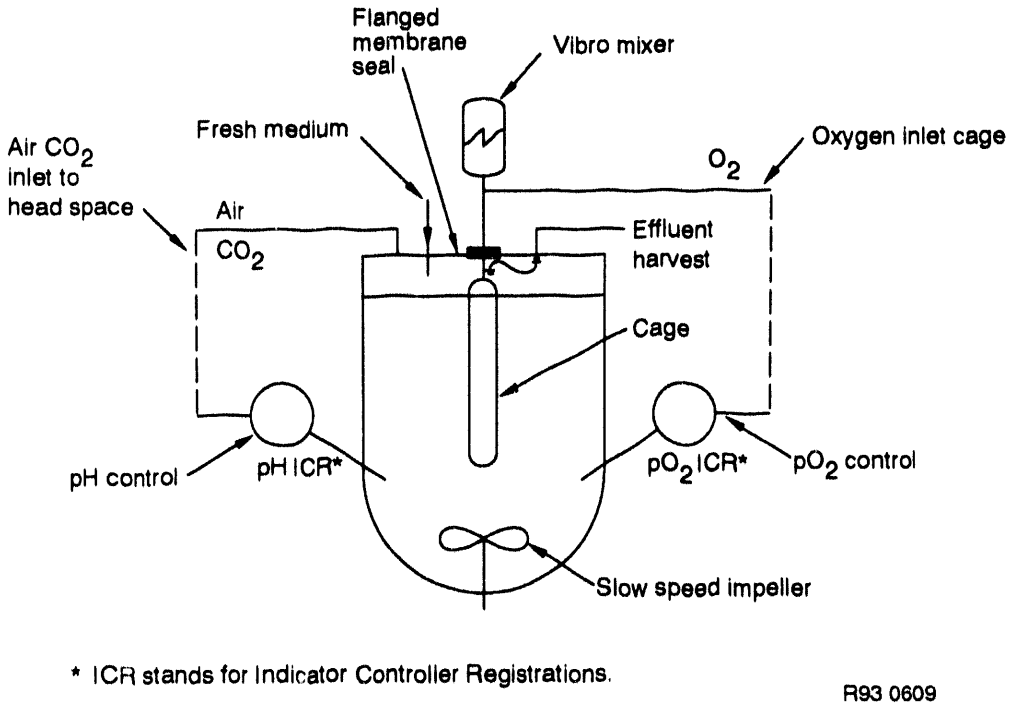

Figure 4. Vibro cage system.

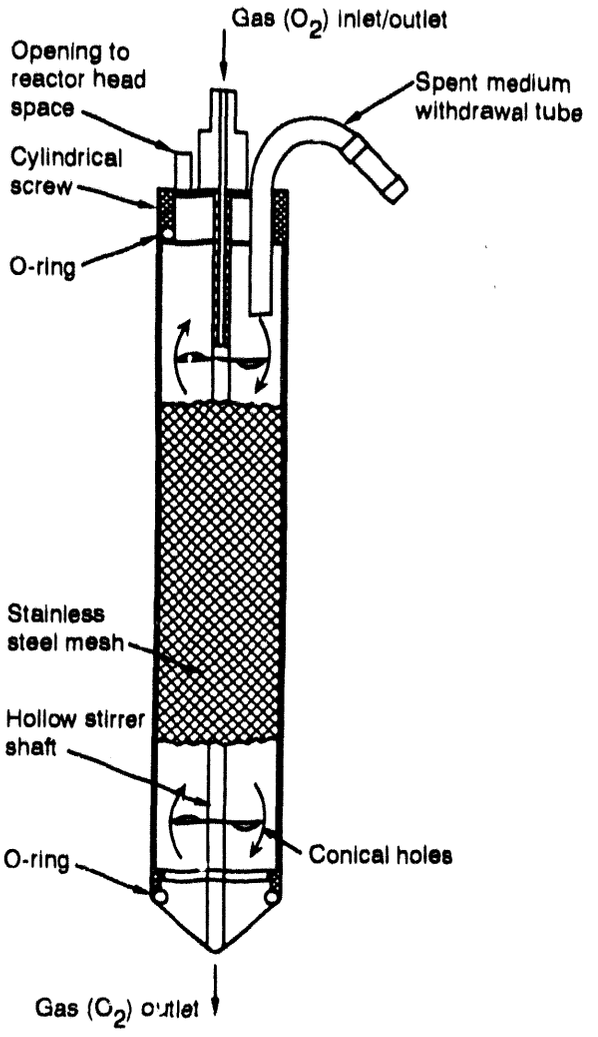

Figure 5. Vibro package.

plugging from the microcarriers and to keep the cage surface clean. Oxygen transfer capacity to cells inside the cage is directly influenced by cage vibration with optimum transfer occurring at an amplitude near 1.0 mm.

Ahmed and Semmens[8] used a microporous hollow fiber membrane with a sealed end to obtain bubbleless aeration of liquid media. Pure oxygen was maintained inside the sealed polypropylene fibers at a pressure below the bubble point allowing oxygen to flow across the hydrophobic membrane and dissolve upon contact with water held outside the membrane. Oxygen transfer efficiency was reported at 100% with an increase in enriched oxygen of up to 30%. Because of the hydrophobic nature of the membrane, oxygen transfer through it is by gas-phase diffusion, which is approximately four orders of magnitude faster than liquid-phase diffusion. Consequently since the overall mass transfer coefficient K, is related to the individual transfer resistances, and gas and membrane resistances are negligible, the following equation:

$$\frac{1}{K} = \frac{1}{Hk_G} + \frac{1}{Hk_m} + \frac{1}{Hk_L} , \qquad (8)$$

can be simplified to:

$$\frac{1}{K} = \frac{1}{k_L} , \qquad (9)$$

where

H = Henry's Law coefficient (atm-L/mg)

k_G, k_M, and k_L = individual mass transfer coefficients (cm/s) of gas, membrane, and water respectively.

Hirasa et al.[9] demonstrated increased oxygen transfer in water with a poly(dimenthysiloxane) hollow fiber membrane (silicone hollow fiber). The inner and outer diameters of the membrane were 0.5 and 1.0 mm respectively. The hollow fiber length was 1,000 cm. Pressures applied to the membrane ranged from $0.98–3.92 \times 10^5$ Pa. The equation used for gas permeation through this homogeneous membrane was as follows:

$$V = P_e(P_1 - P_2)At/L \qquad (10)$$

where

V = gas volume permeated [cm^3 (STP)]

P_e = permeability coefficient [cm^3 (STP) · cm/cm^2 · s · Pa]

P_1 and P_2 = pressures at either side of the membrane (Pa) respectively

A = permeation area of the membrane (cm^2)

t = permeation time (s)

L = thickness of the membrane (cm).

The values of the overall oxygen transfer coefficient were proportional to 0.6 of the surface area of the hollow fiber. In comparison to various types of oxygen utilization systems, the hollow fiber system demonstrated an increase in oxygen enrichment of seven times. Figure 6 shows the relationship between hollow fiber length and oxygen transfer rates.

Gas mass transfer of air was increased by at least five times compared to flat membranes, using a membrane bioreactor featuring pulsating flow past a dimpled membrane.[10] The bioreactor consisted of two hydrophobic polypropylene gas transfer membranes with feed flowing between them. The membranes had a large number of

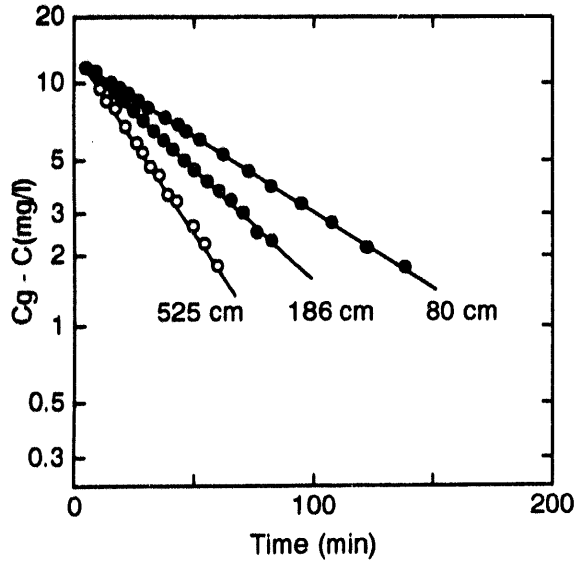

Figure 6. Effect of length of hollow fiber on oxygen transfer from silicone hollow fiber membrane to water.

part-spherical dimples concave to the fluid channel. Pulsatile fluid flow was accomplished with two pistons moving sinusoidally against two pump bags in exact antiphase. The length (l) of the section of the channel (gas permeable) was 160 mm and width (b) was 65 mm. The effective area of a single dimpled membrane was 11,791.8 mm^2. Bioreactor volume was 20 mL, with the addition of end chambers, the end of the membranes and pump bags increased the volume to 120 mL (see Figure 7). Gas was supplied across the back of the membrane with a variable flow air pump. The pulsatile flow across the dimpled membranes caused vortex mixing (see Figure 8) and superior mass transfer compared to flat membranes. The vortex mixing also reduced membrane fouling.

Wu et al.[11] demonstrated increased gas-liquid mass transfer with an airlift bioreactor containing a net draft tube of varying diameters. The system was essentially a bubble column with a diameter 13 cm and 200 cm high with a concentric draft tube 100 cm high of 24 mesh (see Figure 9). The diameter of the tube varied from 6.5, 8.0, 9.0, and 10.4 cm. Increased oxygen mass transfer was demonstrated with the draft tube diameters of 6.5, 8.0, and 9.0 cm as superficial air velocity increased (see Figure 10). Although gas mass transfer decreased with increased pressure, the dissolved oxygen concentration increased in the liquid with increased pressure.

Methane production rates from hydrogen and carbon dioxide were increased with hollow fibers, which allowed methanogens attached on the inside of the hollow fibers to have increased contact with liquid media and gases added from outside the hollow fibers.[12] The cylindrical bioreactor was made of polycarbonate with an inside diameter of 22 mm and 273 mm long, containing 100 hollow fibers of hydrophobic polyethersulfone. The hollow fibers were 273 mm long, with outside diameters of 1.3 mm and inside diameters of 0.8 mm, consisting of a 0.3–0.5 μm pore size. A liquid mineral medium was supplied at a rate of 27 mL/h, with gas (80% H_2 and 20% CO_2) flow through the bioreactor at rates of 1,134, 1,158, and 2,722 mL/h. Methane

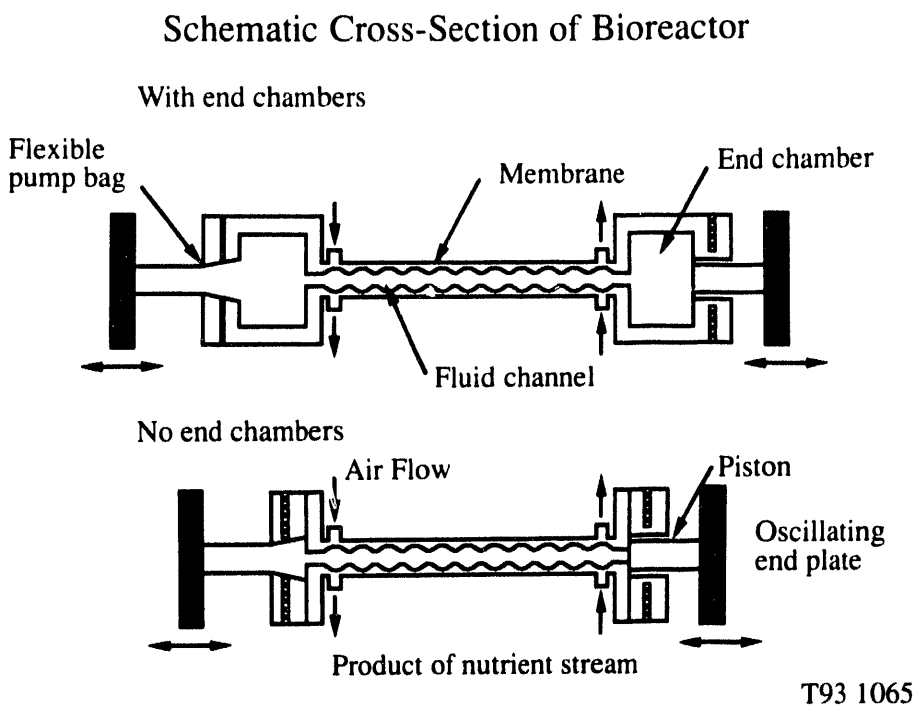

Figure 7. Cross-sectional view of the two bioreactor configurations.

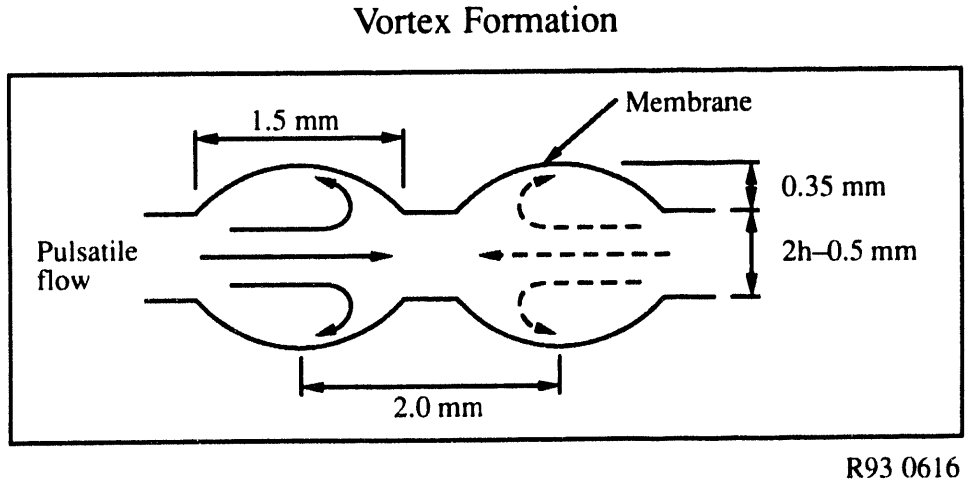

Figure 8. Cross-section showing the spherical geometry of the dimpled membrane.

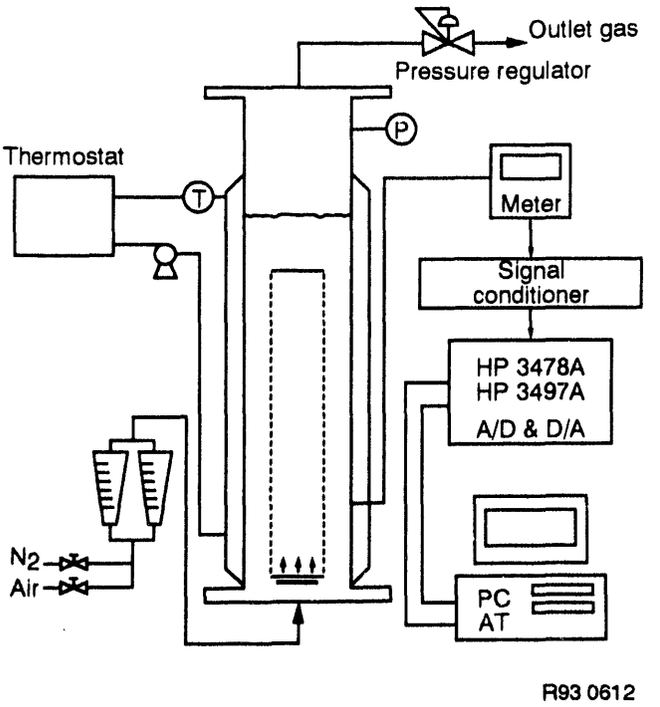

Figure 9. Schematic diagram of the experimental setup of airlift bioreactor with net draft tube.

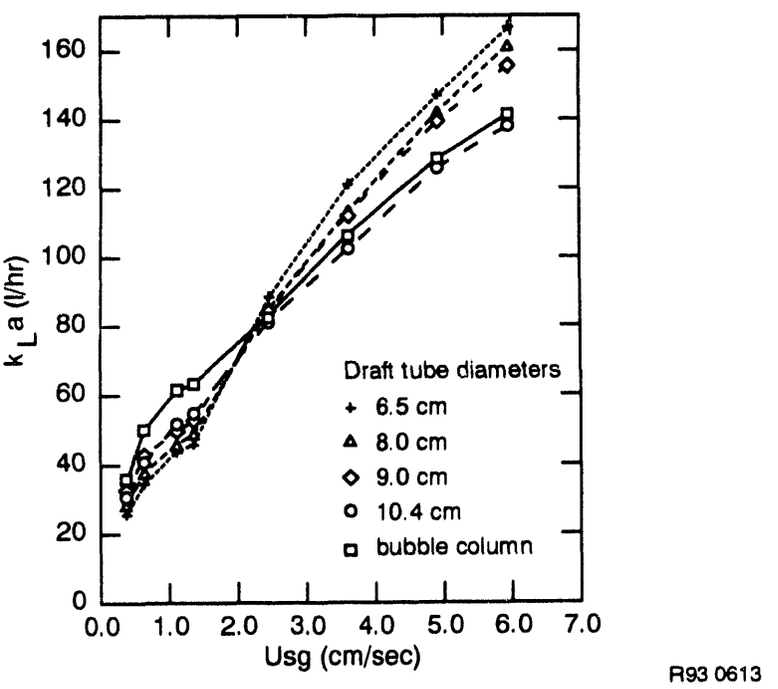

Figure 10. Volumetric mass transfer coefficient with respect to superficial air velocity for different draft tube diameters.

production was proportional to hollow fiber length, with a 90% conversion rate.

Methanogen growth plugged the hollow fibers over time and was overcome by back-flushing of the cells out of the bioreactor with slight positive pressure, leaving the remaining cells to act as the inoculum for the next experiment.

Yano et al.[13] modeled the reaction kinetics of methane production of the above work to design an optimized hollow fiber bioreactor. The following equation was used to solve for the relationship between bioreactor length (l), and the flow rate of H_2, and CH_4 through the bioreactor:

$$l = F_{in}(1 - \varepsilon_H) ln\ [1(1 - Y_h)] + \varepsilon_H \gamma_H\ 0.65\pi y^2 k \qquad (11)$$

where

F_{in} = inlet gas velocity

ε_H = hydrogen flow rate at the inlet over F_{in}

Y_H = conversion of H_2

y = radius to the point of gas limitation

k = reaction rate coefficient.

Apel et al.[14] demonstrated a 90.4% conversion rate of methane using methanotrophs in a gas-phase bioreactor. The methanotrophs were attached to biorings that acted as support for the bacteria while nutrients were added by pumping them to the top of the bioreactor and allowed to trickle down the supports. The microorganisms were in direct contact with the gaseous substrate and therefore minimized diffusional resistance. Additional work by Apel et al.[15] demonstrated increased methane oxidation using 4% kaolin mixed with a mineral salts medium in gas-phase bioreactors. These bioreactors operate similarly to trickle bed bioreactors and therefore the ratio of partial pressures of gaseous reactants entering and leaving the bioreactor can probably be written as:

$$ln \frac{P_S^o}{P_S^i} = \frac{K_L a}{H} \frac{\varepsilon_L h\ RTS}{G} \qquad (12)$$

where

ε_L = fraction of liquid in the column

h = height of the column

S = cross sectional area of the column

R = ideal gas constant

T = absolute temperature

G = gas flow rate.

Applegate and Stephanopoulos[16] used a single-pass, plug-flow bioreactor to supply oxygen to entrapped hybridoma cells via silicone tubes threaded through the square channels of a ceramic monolith. Mean pore size ranged from 20–22 μm with a normal size distribution from 2 – ~150 μm, giving a 50% porosity to the bioreactor. This allowed for a cell concentration in the bioreactor of $>10^8$ cells/cm^3.

The use of a separate oxygenation system created an independent oxygen supply, thereby eliminating the need for rapid recirculation encountered in recycle bioreactors. Since oxygen limiting conditions require rapid recycling, recycling bioreactors are reported to have a very low single-pass substrate conversion rate and can be modeled as a well mixed bioreactor. The bioreactor described here is a single-pass, plug-flow bioreactor (see Figure 11) that can minimize the accumulation of inhibitory metabolic by-products and thereby increase the rate of substrate conversion and produce higher product yields (see Figure 12). This bioreactor permits protection of cells from hydrodynamic effects and has a minimum of moving parts and simplicity of operation when compared to a recycle bioreactor consisting of the same ceramic material.

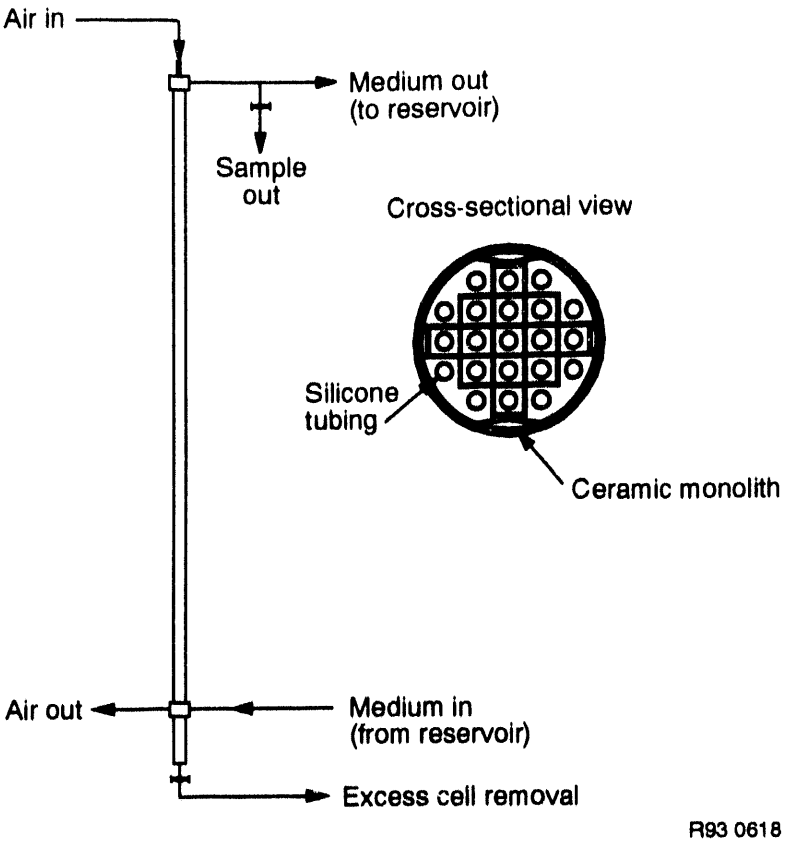

Figure 11. Schematic diagram of single-pass bioreactor.

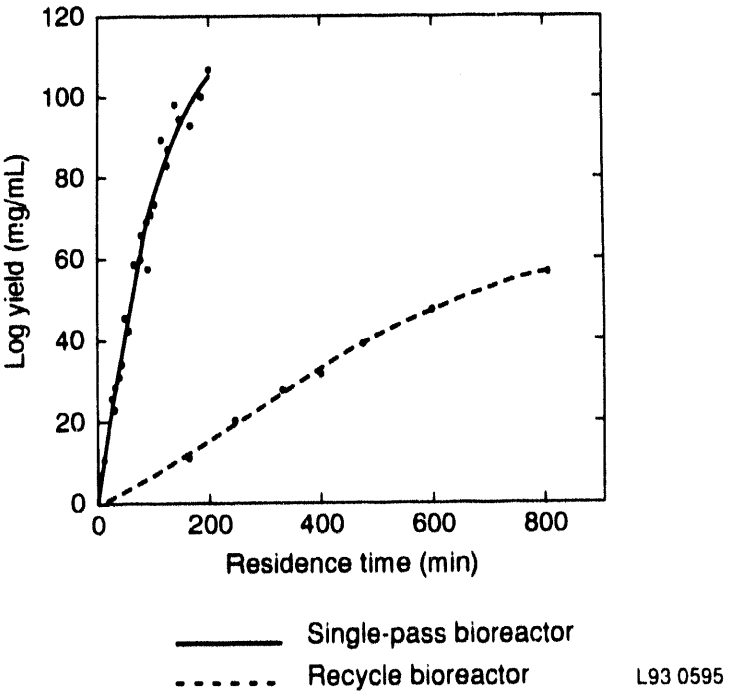

Figure 12. Comparison of antibody yield between the single-pass bioreactor and the recycle bioreactor.

Considerations for scale-up of a single-pass, ceramic matrix bioreactor include effective oxygen diffusivities in liquid and through cell mass, specific oxygen consumption rates, and gas and liquid flow rates. A significant advantage of this bioreactor design involves the high oxygen concentration in the gas phase with minimum oxygen depletion occurring because of axial diffusion. From the cross-sectional diagram of one channel (Figure 13), liquid flows in the z-direction while oxygen diffuses from the gas phase through the tubing wall, across the open channel, and into the porous wall where it is consumed by entrapped cells.

Oxygen mass transport in this system is governed by the following equations:

$$\underline{v}(\nabla c) = D\nabla^2 C \qquad (13)$$

$$D_W \nabla^2 c_W = S_v \qquad (14)$$

where

$\underline{v}$ = velocity field of liquid flowing through the open channel

c = oxygen concentration in the channel

c_W = oxygen concentration in the porous wall-cell mass composite

D and D_W = effective oxygen diffusivities through liquid and the porous wall-cell mass composite

S_v = a uniform volumetric oxygen consumption rate (0 order kinetics).

Equation 13 refers to the open channel between the silicone tubing and the porous wall, while Equation 14 describes oxygen diffusion and consumption by cells immobilized in the porous wall.

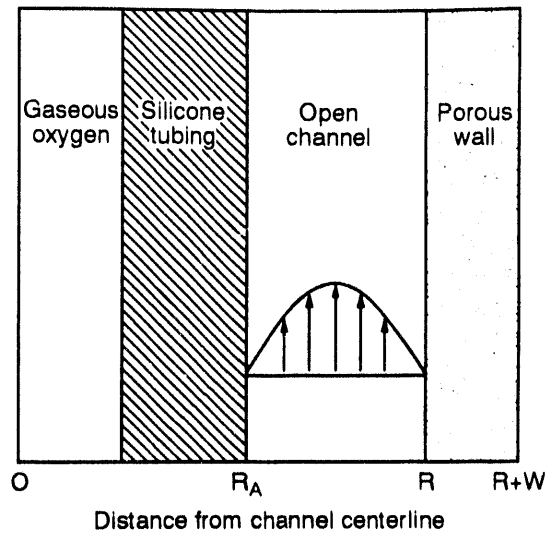

L93 0603

Figure 13. Cross-sectional view of single-pass bioreactor as formulated in the oxygen transport model.

Equations 13 and 14 are coupled through boundary conditions at the channel-porous wall interface, while other boundary conditions are imposed at the tubing wall-channel interface and the inlet to the bioreactor. These boundary conditions are as follows, assuming fully developed flow at the entrance and a flat profile for the gas-phase concentration of oxygen in the tubing:

$$c = c_T \text{ at } y = R_A \qquad (15)$$

$$c = c_W \text{ at } y = R \qquad (16)$$

$$-D\left(\frac{dc}{dy}\right) = -D_W\left(\frac{dc_W}{dy}\right) \text{ at } y = R \qquad (17)$$

$$\frac{dc_W}{dy} = 0 \text{ at } y = R + W \qquad (18)$$

$$c = c_L \text{ at } z = 0 \qquad (19)$$

where

z = axial position along the bioreactor

y = transverse position across the channel and porous wall

R_A = distance between the channel centerline and outer tubing wall

R = half-channel width and corresponds to the interface between the medium and the porous wall

W = half-wall thickness

c_T = liquid-phase oxygen concentration at the tubing wall-fluid interface

c_L = inlet liquid-phase oxygen concentration.

In order to optimize bioreactor scale-up, equations were developed relating to design variables such as bioreactor length and wall thickness to operating variables such as gas flow rate and oxygen consumption rate. The design criteria developed were based on maintaining a minimum oxygen concentration throughout the bioreactor. The minimum oxygen concentration occurs at the midsection of the porous wall, and its value depends on the dissolved oxygen concentration at the tubing wall-liquid interface, c_T, as follows:

$$C_{w,min} = C_{T,min} + \left(\frac{S_v R^2}{4D_w}\right)\left\{\left(1 + \frac{W}{R}\right)^2 \times \left[1 - 2\ln\left(1\ \frac{W}{R}\right)\right]\right\} - S_v \frac{W^2}{2D}\left[2\left(\frac{R}{W}\right) + 1\right]\ln\left(\frac{R_A}{R}\right) \qquad (20)$$

where

$c_{w,min}$ = dissolved oxygen concentration at the wall midsection.

The rate of oxygen supplied to the culture in this bioreactor design will limit bioreactor scale-up. The following equation determines the minimum gas flow rate required by formulating a mass balance on the tube side oxygen supply, based on an acceptable $c_{t,min}$:

$$F_{min} = \frac{S_{vL}\pi[(R + W)^2 - R^2]}{C_g - Hc_{t,min}} \qquad (21)$$

where

c_G = inlet gas phase O_2 compositions

c_w = dissolved oxygen concentration at the wall midsection.

F = gas flow rate through each tube

H = Henry's Law coefficient for O_2 in medium. Oxygen permeability through silicone was not considered in the above equation, however.

Another method to increase the oxygen supply to cells is to increase gas flow rates through the tubing so that the transverse oxygen profile at the bioreactor exit is maintained above a minimum value throughout the porous wall. Maximum flow rate is determined by the maximum pressure drop the tubing can sustain. Therefore maximum bioreactor length can be determined in the following way:

$$L_{max} = \left\{\frac{|\Delta p|_{max} D_i^4}{128\mu S_v}\left[\frac{C_G - C_{T,min}}{(R + W)^2 - R^2}\right]\right\}^{1/2} \qquad (22)$$

where

$|\Delta p|_{max}$ = maximum pressure drop the tubing can sustain

μ = gas viscosity

D_i = inner tubing diameter.

Since gases are more soluble in water at increased pressure, bioreactors designed to operate at increased pressures have been successful in increasing bacterial growth rates. Numerous bioreactor designs have been developed for this purpose and can operate at pressures up to 700 atmospheres. Nelson et al.[17] demonstrated that bacterial growth rates can vary at increased pressure based on whether hyperbaric or hydrostatic pressures are used (see Figure 14). Hydrostatic pressurization offers the advantages of easy pressure control and safety, but the effectiveness of these systems is limited when gaseous

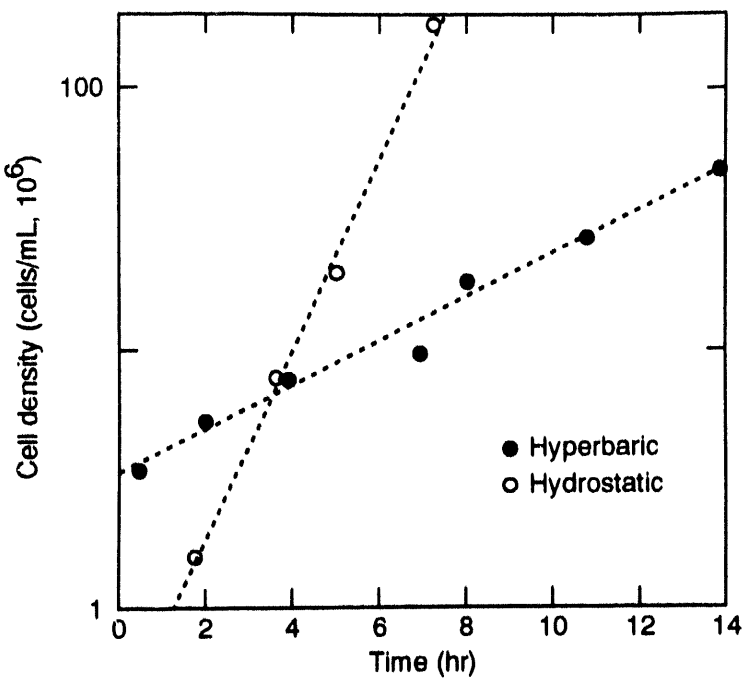

Figure 14. Growth of ES4 at 95°C and 500 atm in the hydrostatic vessel and the glass-lined hyperbaric vessel.

substrates are involved. A bioreactor used to compare effects of hyperbaric and hydrostatic pressures on bacterial growth is shown in Figure 15.[17] A modified high-pressure bioreactor system was modified to allow hyperbaric studies to be conducted in parallel with hydrostatic experiments.

Enhanced oxygen transfer rates have been accomplished with chemical additives acting as oxygen vectors. In these chemicals, oxygen has a high solubility, and when combined with water allows the medium to carry more oxygen. Chemicals commonly used in biotechnology include hydrocarbons, hemoglobin, and perfluorocarbons. Hydrocarbons are inexpensive and can be separated by decantation or centrifugation.

Torrijos[18] demonstrated increased growth kinetics with n-alkanes. Disadvantages of n-alkane use include damage to cell membranes and potential microbial oxidation.

Adlercreutz and Mattiason[19] used hemoglobin as an oxygen carrier for *Gluconobacter oxyddans* with increased growth and productivity. Although hemoglobin proved successful, the upper limit of use was demonstrated at 85 mg/mL. Recycling of hemoglobin must be accomplished with ultrafiltration, requiring the need for immobilized cells to be used with soluble hemoglobin. Hemoglobin was oxidized to methemoglobin, thereby decreasing its oxygen carrying capacity. Khosla and Bailey[20] overcame some of the problems in working with hemoglobin by cloning the hemoglobin gene into *Escherichia coli*, producing increased growth rates and oxygen utilization.

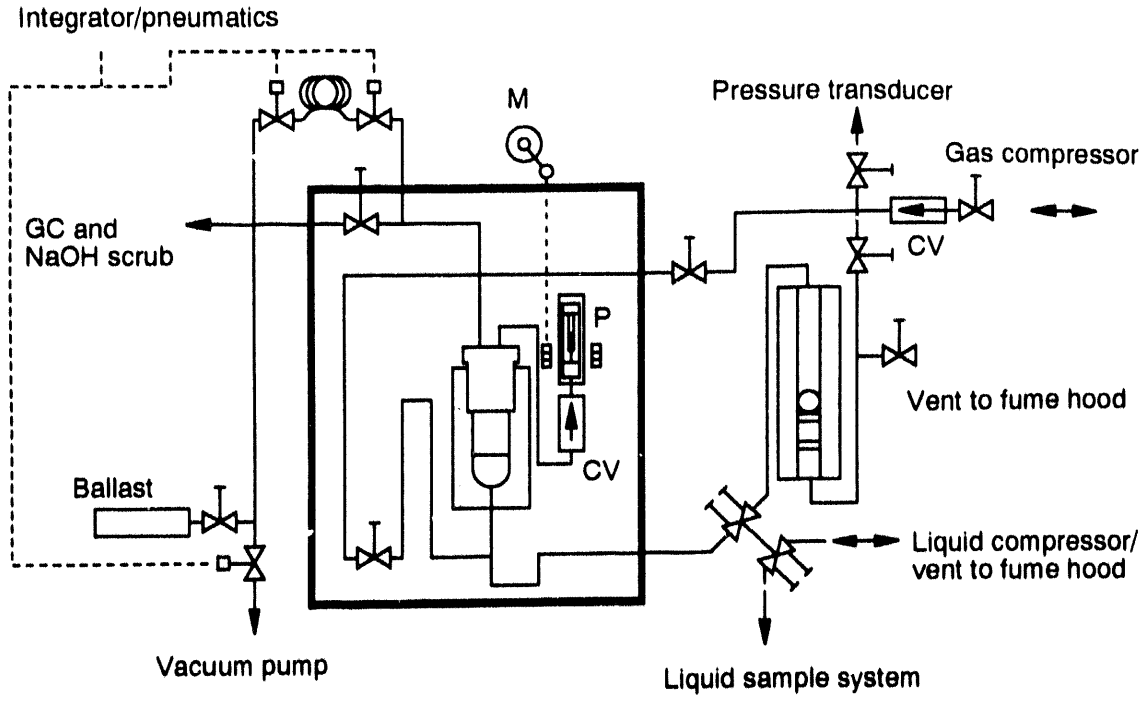

CV – Check valves

P – Gas recirculation pump

M – Motor driven crank

GC – Gas chromatograph

Figure 15. Schematic diagram of modified high-pressure system.

Perfluorocarbons are hydrocarbons with the hydrogens replaced with fluorine molecules. Their gas dissolving capacity is related to the ease in which solute molecules can fit in between the fluorine molecules[21] rather than a specific chemical reaction. Much of the research pertaining to perfluorocarbons as oxygen carriers has been reviewed by Rols[21] and King et al.[22] Perfluorocarbons have been demonstrated as suitable blood substitutes and have improved the productivity of aerobic microorganisms. Because of their high cost (~350 – $400 per gallon), they would need to be recycled in any bioprocess in which they are used. Dammiano and Wang[23] recycled perfluorocarbons in a spray column bioreactor by removing the perfluorocarbons from the bottom of a cylindrical bioreactor where they settled and pumping them back through the system by means of aspiration after they were reoxygenated outside the bioreactor (see Figure 16). Because of the high volatility of many of the perfluorocarbons, a means of trapping them needs to be in place such as that used by Damianno and Wang,[23] where a refrigerated trap was used to condense any escaping perfluorocarbons from the system (see Figure 16). Perfluorocarbon emulsions have also been used with better results than the liquids, because of their ability to remain in suspension and have more contact time with the microorganisms in the media.

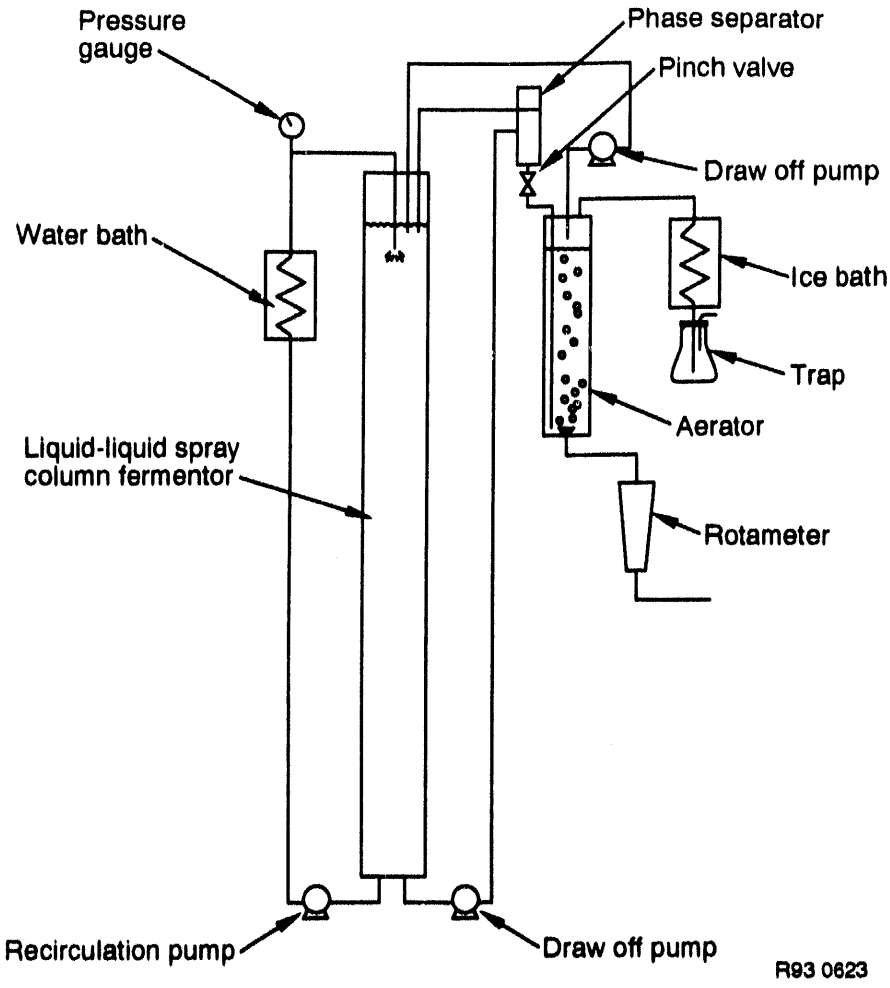

Figure 16. Schematic of liquid-liquid spray column fermentor system.

Ju et al.[24] have investigated the use of perfluorocarbon emulsions and developed a model to describe their potential oxygen enhancement effects in liquid media. The model is as follows:

$$E = \left[\left(\frac{P_e}{P_o}\right)\left(\frac{k_e}{k_o}\right)\right]^{1/2} \quad (23)$$

where

E = oxygen transfer enhancement factor

P_e and P_o = oxygen permeability [(mol · cm^2/(L·s·atm)] of the effective value in a homogeneous system and the original value, respectively

k_e and k_o = effective and original values of oxygen solubility in terms of Henry's law constant [(mol/(L·atm)].

Gases other than oxygen are also soluble in perfluorocarbons. King et al.[22] suggested a possible use of perfluorocarbons in microbial culture as carriers of other metabolically important gases. Perfluorocarbons enhanced the growth of *Clostridium perfringens* when grown with carbon dioxide.[25] Ju and Armiger[24] used perfluorocarbons to remove carbon dioxide from aerobic microbial cultures.

Perfluorocarbons also have several other characteristics that may make them potentially more valuable in bioprocessing, including (a) nonbiodegradability, (b) enhanced solubility of numerous hydrocarbons, (c) high electrical conductivity, and (d) low surface tension. Some of these characteristics are detailed in Tables 1 and 2.

Table 1. Typical properties of fluorocarbons.

English
Metric

Flourinert Liquids	Typical Boiling Point °F °C	Pour Point °F °C	Density, 25°C lb/ft3 g/cm3	Density, -54°C lb/ft3 g/cm3	Kinematic Viscosity, 25°C cs	Kinematic Viscosity, -54°C cs	Vapor Pressure, 25°C lb/in2 torr	Specific Heat, 25°C Btu/lb - °F g - cal/g - °C	Heat of Vaporization @ Boiling Point Btu/lb g - cal/g	Thermal Conductivity, 25°C Btu/(hr) (ft2) (°F/ft) watts/(cm2) (°C/cm)
FC-87	86 30	-150 -101	102 1.63	115 1.84	0.4	1.1	11.80 610	0.25	38 21	0.032 0.00055
FC-72	133 56	-130 -90	105 1.68	119 1.90	0.4	1.9	4.49 232	0.25	38 22	0.033 0.00057
FC-84	176 80	-139 -95	108 1.73	120 1.93	0.55	4.0	1.53 79	0.25	35 19	0.035* 0.00060*
FC-77	207 97	-139 -95	111 1.78	123 1.97	0.8	6.9	0.812 42	0.25	36 20	0.036* 0.00063*
FC-104	214 101	-85 -65	110 1.77	122 1.96	0.8	7.3	0.560 29	0.25	40 22	0.036* 0.00063*
FC-75	216 102	-126 -88	110 1.77	122 1.95	0.8	7.4	0.600 31	0.25	38 21	0.036 0.00063
FC-40	311 155	-70 -57	117 1.87	— —	2.2	—	0.058 3	0.25	31 17	0.038* 0.00065*
FC-43	345 174	-58 -50	117 1.88	— —	2.8	—	0.025 1.3	0.25	30 17	0.038 0.00066
FC-70	419 215	-13 -25	121 1.94	— —	14.0	—	<0.002 <0.1	0.25	29 16	0.040* 0.00070*
FC-5312	419 215	-13 -25	120 1.93	— —	12.6	—	<0.002 <0.1	0.25	29 16	0.040* 0.00070*

* Estimated values

— Not measured due to relative proximity to pour point

T93 1066

Table 1. (continued).

Coefficient of Expansion ft³/(ft³) (°F) Cm³ (cm³) (°C)	Surface Tension, 25°C poundals/in dynes/cm	Refractive Index, 25°C	Dielectric Strength, 25°C KV (0.10 in gap) KV (2.54 mm gap)	Dielectric Constant, 25°C (1 KHz)	Dissipation Factor, 25°C (1 KHz)	Volume Resistivity, 25°C ohm - cm	Solubility of Water @ 25°C ppm (wt.)	Solubility of Air @ 25°C in³ gas/100 in³ liquid ml gas/100 ml liquid	Average Molecular Weight	Flourinert Liquids
0.0009 0.0016	0.0018 9.5	1.238	42	1.72	<0.0005	—	—	—	290	FC-87
0.0009 0.0016	0.0022 12	1.251	38	1.76	<0.0003	1.0×10^{15}	10	48	340	FC-72
0.0008 0.0014	0.0024 13	1.261	42	1.81*	<0.0003*	1.0×10^{15}*	11*	43*	388	FC-84
0.0008 0.0014	0.0028 15	1.280	40	1.86	<0.0003	1.9×10^{15}	13	41	415	FC-77
0.0008 0.0014	0.0026 14	1.271	41	1.86	<0.0001	8.4×10^{15}	11	38	435	FC-104
0.0008 0.0014	0.0028 15	1.276	40	1.86	<0.0001	8.0×10^{15}	11	40	420	FC-75
0.0007 0.0012	0.0029 16	1.290	46	1.89	<0.0003	4.0×10^{15}	7	27	650	FC-40
0.0007 0.0012	0.0029 16	1.291	42	1.90	<0.0001	3.4×10^{15}	7	26	670	FC-43
0.0006 0.0010	0.0033 18	1.303	40	1.98	<0.0001	2.3×10^{15}	8	22	820	FC-70
0.0006 0.0010	0.0033 18	1.303	40	1.98	<0.0001	2.3×10^{15}	8	22	820	FC-5312

T93 1067

Table 2. Some properties of the unwoven fibrous packing materials.

Fabrics	Composition	Elemental analysis					pH	Moisture content, %	Specific surface area, $m^2.g^{-1}$
		C	H	N	S	Ash			
Rayon	Rayon	42.5	6.5	0	0	0	6.1[b]	8.78	242[d]
Polyester	Polyester	62.2	4.5	0	0	0.6	5.4[b]	0.91	33[d]
Acryl	Acrylic	67.9	5.9	26.9	0	0	5.2[b]	0.95	<3[d]
Asgard	Activated carbon fabric made from rayon	56.8	3.7	4.4	0.4	7.3	2.61[b]	8.52	504[d]
FN-200CF-15	Carbon fiber (20%) + fibrous charcoal (80%)[a]	91.4	0.5	0.6	0	0.4	5.53[c]	4.98	1,200[e]
FN-150PE-15	Polyester (30%) + fibrous charcoal (70%)	86.0	3.9	0.3	0	0	5.36[c]	3.18	1,050[e]
FN-300PS-15	Fibrous charcoal (100%)	89.2	0.8	0.4	0.1	0.2	5.28[c]	1.95	1,500[e]
FN-300PP-15	Polypropylene (10%) + fibrous charcoal (90%)	70.4	1.2	0.2	0	0	4.84[c]	17.7	1,350[e]
FN-200AC	Polyacrylonitrite	65.7	2.0	4.0	0.3	1.6	5.49[c]	21.8	562[d]

a. Surface area of the fibrous charcoal is 1,500 $m^2.g^{-1}$.

b. 1:19 (fab.:water) ratio (see text).

c. 1:39 (fab.:water) ratio (see text).

d. The values were measured by the determination of pore volume distribution by methyl alcohol isotherm method (7).

e. The values were calculated from fibrous charcoal content of the fabrics.

VOC REMOVAL

Several bioreactor designs have been reported for removing VOCs from gas streams. A successful bioreactor design needs to solve the problems of oxygen usually being required for the rapid metabolism of VOCs and the immiscible nature of VOCs with water. These problems are usually addressed by increasing the surface area inside the bioreactor with a solid support medium. Support media selection depends on good pneumatic conductivity to minimize pressure drop and gas movement power requirements, as well as high surface area and good wetting sorptive characteristics. These media allow for increased surface area for bacterial growth, oxygen transfer, and increased sorption for hydrophobic VOCs such as gasoline and diesel fuel.

Bioreactors similar in design to those of Apel[14,15] mentioned earlier, (see Figure 17) were used by Douglass et al.,[26] (see Figure 18). Various packings were identified as better solid media and included; soil, peat, and fiberglass wool. Other packing media used in the biological removal of VOCs were composts, sand, bark peat, heather, volcanic ash, or mixtures of these.[27] Tiwaree et al.[28] used different fabrics (see Table 2) as carriers of microorganisms in the biological deodorization of dimethyl sulfide. Employing the bioreactor design outlined in Figure 19 they found the activated carbon fabric FN-200CF-15 had the highest rate of substrate removal (see Table 3) following an acclimation period in the bioreactor. The results of bacterial counts from the fabrics, using three different media (see Table 4), demonstrated that fabric FN-200CF-15 also had the highest bacterial density (see Table 5). Advantages of this particular fabric over the others tested include light weight and flexibility, less degradable, and it had a relatively higher surface area providing for broader environmental conditions for microbial growth. Lee and Shoda[29] also found that unwoven fabrics outperform fibrous fabrics in the removal of methanethiol.

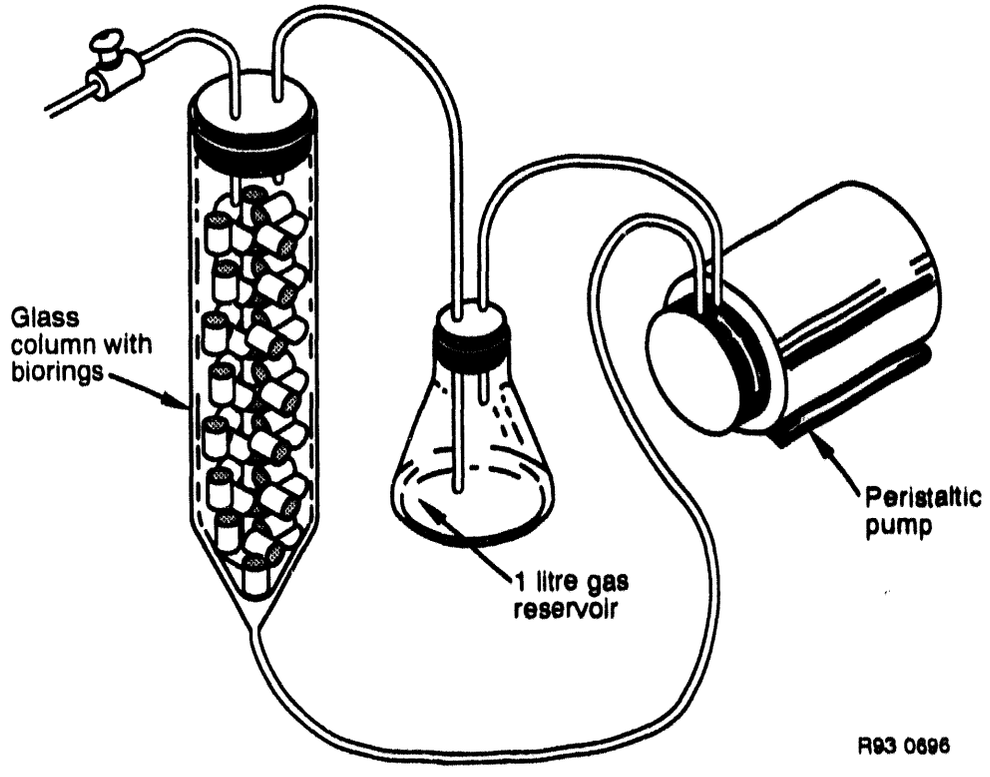

Figure 17. Schematic diagram of gas phase bioreactor.

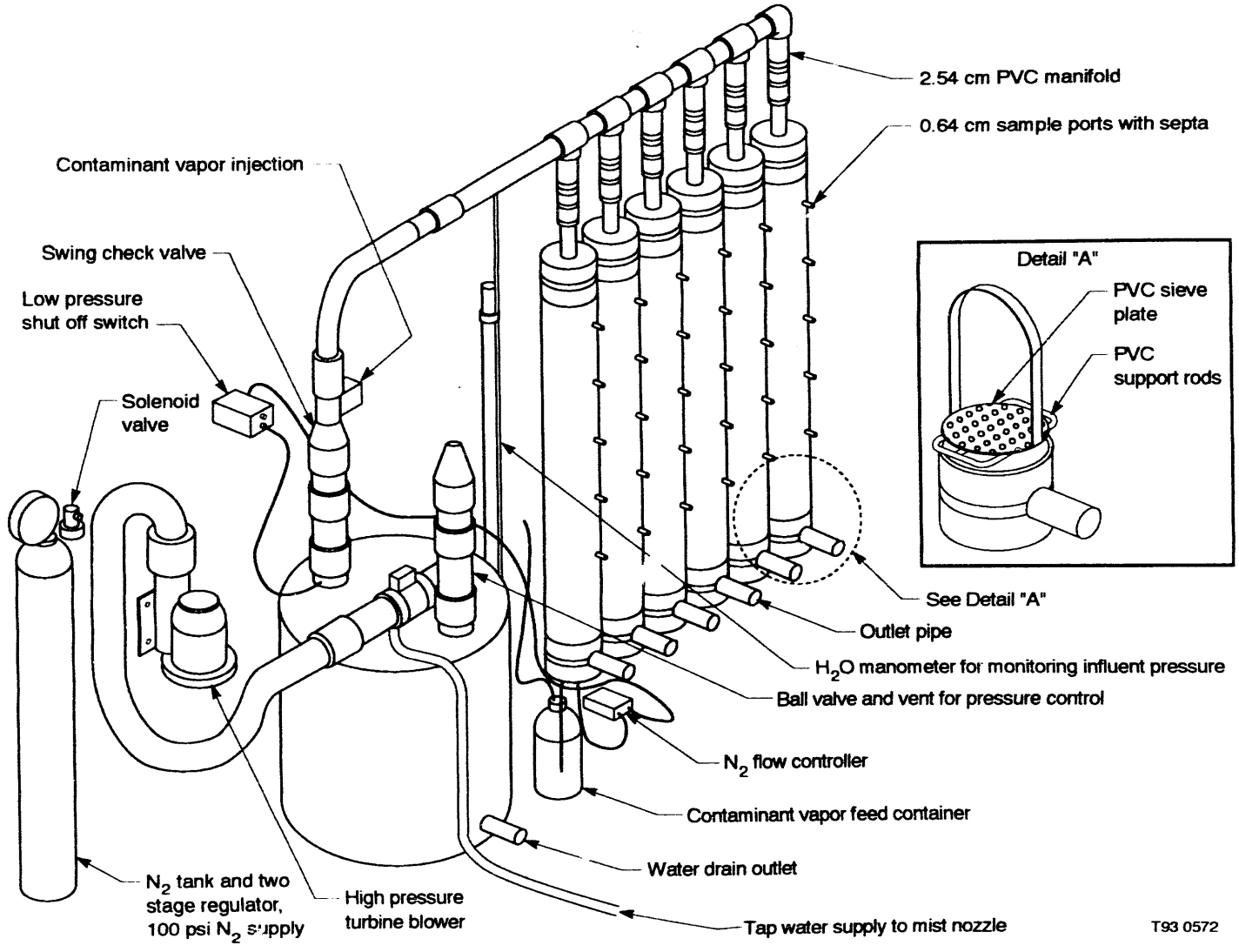

Figure 18. Bioreactor test system.

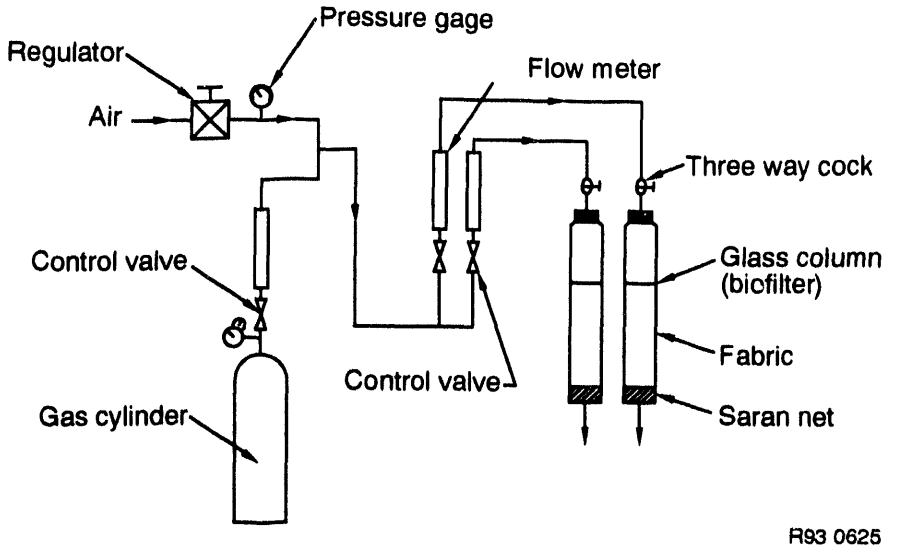

Figure 19. Schematic diagram of the laboratory-scale fabric biofilter system.

Table 3. Maximum removal rates of DMS in different fabric biofilters.

Packing materials	Parameters	
	V_m[a]	K_s[b]
Rayon	0.50	3.67
Acryl	0.45	3.14
Polyester	0.83	1.83
Asgard	1.33	8.68
FN-200CF-15	2.28	6.28
FN-200AC	1.16	5.80
FN-300PP-15	1.08	6.27
FN-300PS-15	0.64	2.91
FH-150PE-15	0.66	3.24
Peat (2)	0.38	10.00
Polypropylene (6)	0.34	3.40
Nylon (6)	0.47	4.10

a. U; g-S/kg-dry fab./d.

b. U; ppm.

Table 4. Compositions of media used for bacterial countings.

Name of media	MW		DMSO		Nutrient-agar	
Compositions	KH_2PO_4	3	K_2HPO_4	1.55	$Na_2HPO_4.12H_20$	2
(g/L)	NH_4Cl	0.1	NaH_2PO_4	0.85	NaCl	3
	$MgSO_4.7H_2O$	0.5	$(NH_4)_2.SO_4$	0.1	Yeast extract	3
	$CaCl_2.2H_2O$	0.3	NH_4Cl	2	Meat extract	3
	$FeSO_4.7H_2O$	0.01	$FeSO_4.7H_2O$	0.01	Peptone	15
	$Na_2S_2O_3.5H_2O$	8	Yeast extra	0.1	Agar	20
	Gellan gum	5	DMSO[a]	1		
			Gellan gum	5		

a. U; mL/L.

Table 5. Bacterial counting in different media.

	Media (cfu/dry-fab.)[a]		
Packing materials	DMSO	MW	NA
Rayon	1.7×10^8	1.05×10^8	5.1×10^7
Acryl	4.1×10^8	3.52×10^8	4.1×10^8
Polyester	4.42×10^8	3.89×10^8	4.15×10^8
Asgard	3.25×10^8	2.84×10^8	2.27×10^8
FN-200CF-15	8.76×10^9	1.29×10^{10}	8.64×10^9
FN-200AC	2.64×10^9	2.87×10^9	ND[b]
FN-300PS-15	3.47×10^9	2.45×10^9	2.04×10^9
FH-150PE-15	2.99×10^9	2.11×10^9	1.32×10^9
FN-300PP-15	1.96×10^9	2.85×10^9	ND[b]

a. Colony forming units/dry fabric.

b. Not determined.

SOLVENT DEGRADATION

Numerous organic solvents have been identified as soil and water contaminants. The route of travel from soil is either via volatilization or entry into the ground water. Several physical techniques for vapor removal from soil and water involve vapor-phase extraction or gas stripping. Both methods remove volatiles from soil and water by transferring them to air via decreased pressure. After transfer into the gas phase, volatilized organic compounds can be treated biologically using methods discussed in previous sections. Solvent removal from contaminated water is complicated by the immiscibility of most solvents in water as well as potential toxic effects on microorganisms at high concentrations. Gas phase and trickling filters are commonly used as bioreactor designs because of their increased surface area, thus allowing increased mass transfer.

Many chlorinated solvents can be degraded by methanotrophic bacteria because of their ability to cometabolize these chemicals with methane. Methane however remains a preferred substrate and can reduce the degradation rates of solvents through competitive inhibition. Although methane is needed for enzyme induction, Speitel and Leonard[30] have used methanotroph physiology in developing a sequencing biofilm bioreactor that minimizes competitive inhibition from methane and increases chlorinated solvent degradation rates. The bioreactor design employs two modes of operation consisting of a growth mode and a degradation mode. During the growth mode (see Figure 20), methane and oxygen were supplied in

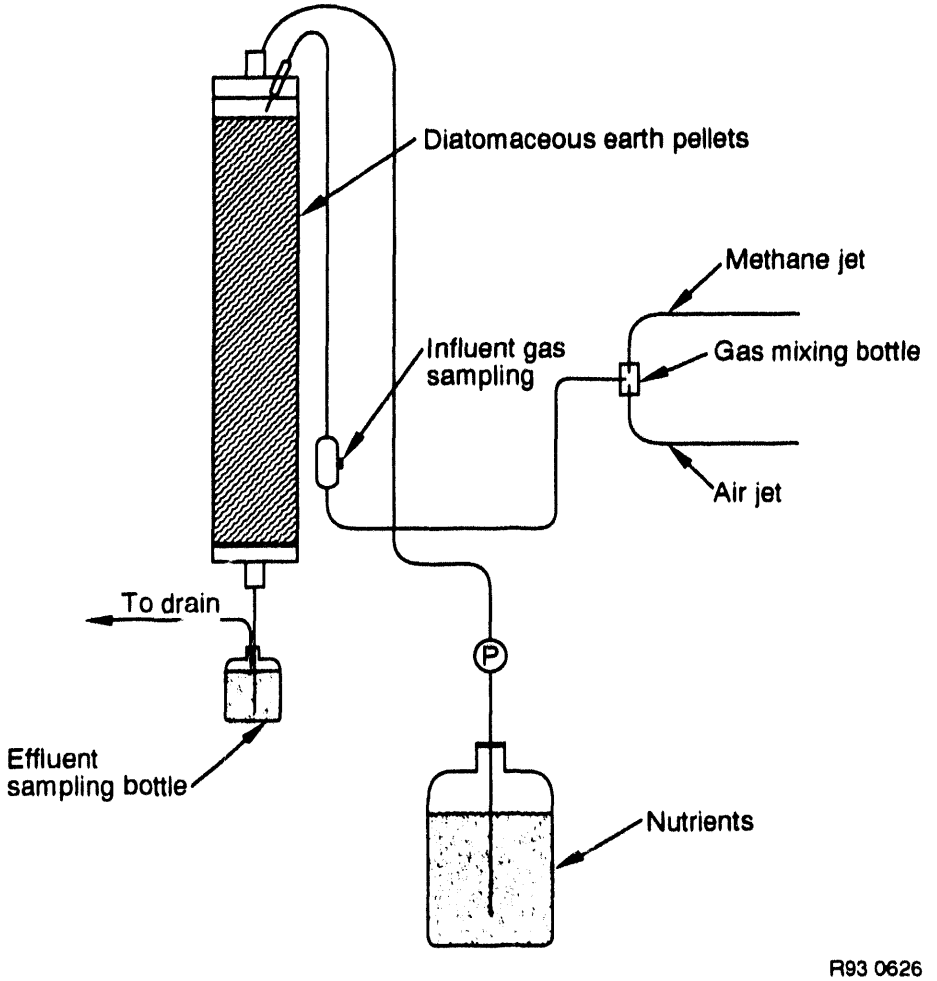

Figure 20. Schematic of sequencing reactor during growth mode.

the gas phase to the organisms. This allowed for increased biomass in the bioreactor and induction of nonspecific enzymes essential for solvent degradation. The degradation mode (see Figure 21) involved filling the bioreactor with water containing formate as a source of energy for chemical reducing power, and chloroform as a model chlorinated compound. Although this bioreactor design and operation have not been optimized, the authors demonstrated significantly better results with the sequencing bioreactor than a packed-bed, continuous flow bioreactor, due primarily to the increased biomass permitted in the sequencing bioreactor.

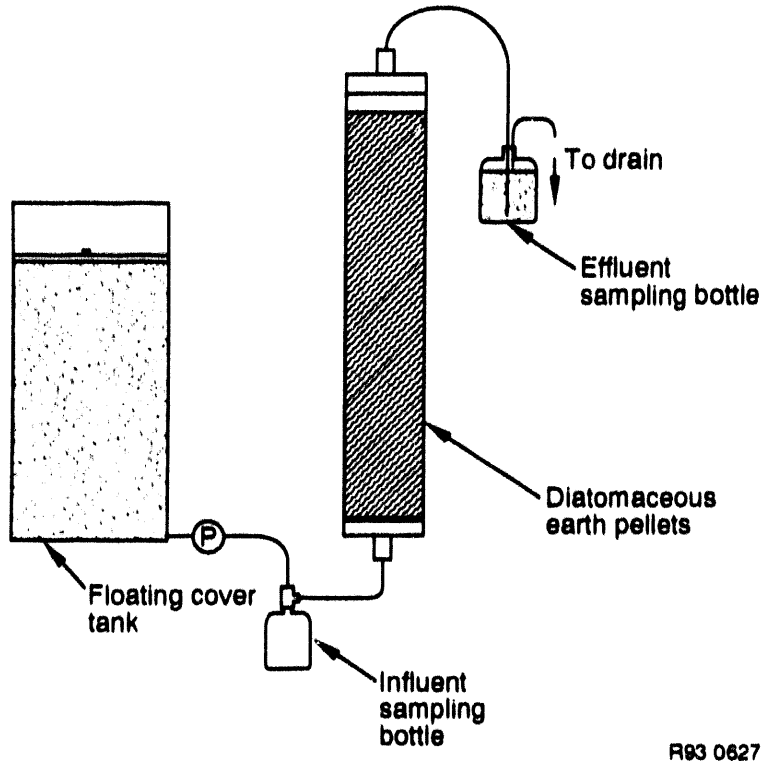

Figure 21. Schematic of sequencing reactor during degradation mode.

CELL IMMOBILIZATION STRATEGIES

In order to operate bioreactors at high dilution rates and separate cells from by-products, immobilized cell technologies have been employed in numerous situations. These techniques can be categorized into two general groups: cells attached to a solid support medium, thereby forming a biofilm; and cells (or enzymes) embedded into a solid or semisolid matrix such as gel beads. Important properties of support media include porosity, leaching ability, and surface roughness.

Problems associated with immobilized cell bioreactors include:

- Clogging caused by increased cell biomass
- Unstable bed expansion caused by imbalanced cell growth
- Accumulation of dead cell mass
- Gas entrapment inside the bioreactor
- Nutrient channeling as in trickle bed bioreactors
- Cell leakage of gel disintegration associated with immobilized cells in gel beads.

Lewis and Yang[31] have demonstrated a packed bed bioreactor for continuous propionic acid fermentation employing a spiral wound, fibrous bed bioreactor (see Figure 22). The cells, *Propionibacterium acidipropionici* ATCC 4875, were attached to the fibers and entrapped in the void volume inside the matrix of the material. The fibrous material was made from a piece of cotton towel, overlaid with stainless steel mesh. This matrix was spirally wound around the vertical axis with a 5 mm gap between layers and placed in a glass column on top of ceramic supports. Void volume was approximately 90%. Bacterial density approached 37 g/L, while productivity of this bioreactor approached four times that of batch systems for 4 months without problems from contamination, clogging, or degeneration.

A number of solid supports, including baked clay and melted slug were used for methanogens by Nishio et al.[32] to retain the cells in bioreactors fed acetate and formate for increased methane production efficiency. Hydraulic retention times were shortened from 18 h in chemostat culture to 0.4 h in fixed bed culture with formate and 6.71 days to 0.15 days with acetate (see Table 6).

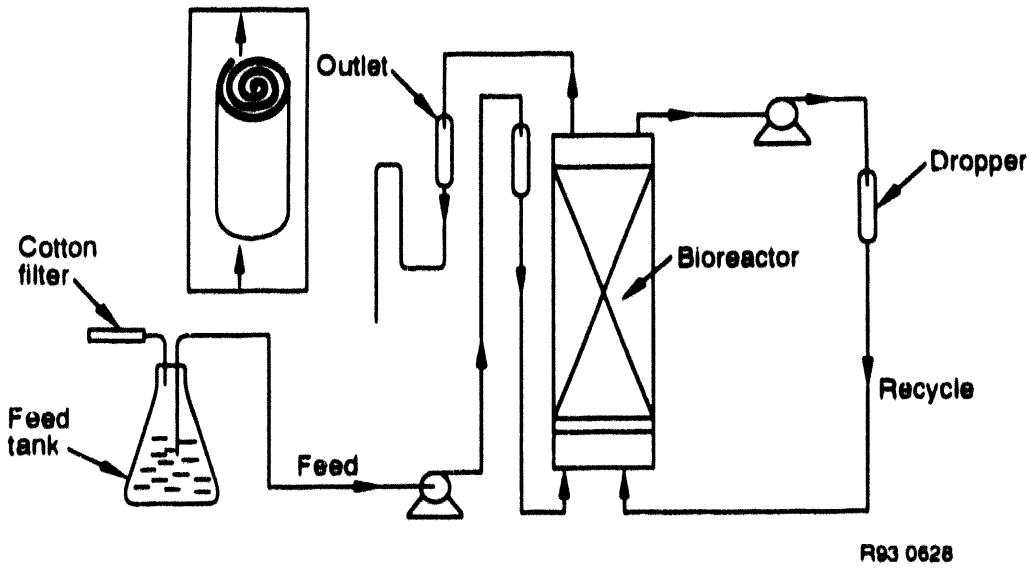

Figure 22. Experimental packed bed bioreactor apparatus.

Table 6. Methane fermentation from formate in fixed-bed reactor.[a]

Support material	Formate consumption rate (mmol/L-day)	Methane production rate (mmol/L-day)	Hydraulic retention time (h)	Cell concentration (g/L)	Methane yield (mol/mol)
Zeolite No. 3	3,587	639	0.7	19.2	0.18
Glass beads	96	20	4.6	NT[c]	0.22
Baked clay	6,717	1,720	0.4	20.1	0.26
Melted slug	4,065	1,010	0.6	14.9	0.25
Cellulose acetate fiber	1,870	475	1.7	5.80	0.26
Activated carbon fiber	1,761	380	1.5	5.81	0.22
Sponge rubber	213	14	4.1	ND[c]	0.06
None[b]	161	37	18	0.07	0.23

a. Steady state data obtained at a nearly critical dilution rate.

b. Chemostat culture without fixed bed.

c. Not determined.

Porous microcarriers for methanogens (see Table 7) when compared to sand were shown by Yee et al.[33] to be superior in their cell retention capacity (see Table 8) because of increased surface area, total pore volume, and mean pore diameter, thereby increasing bioreactor efficiency and decreasing startup time.

Penicillinase and lactate dehydrogenase were immobilized in a ceramic membrane microfilter constructed from alpha alumina particles.[34] The substrate solution permeated the membrane and reacted with the enzymes inside. Figure 23 demonstrates how the bioreactor was operated, where S_T, V_R, and V_T are reservoir concentration, bioreactor volume, and reservoir (tank) volume, respectively. Neither mass transfer effects or shear effects were observed during operation of this bioreactor. This bioreactor design may be desirable when an immobilized enzyme has a high activity and a low Michaelis constant.

Glucoamylase was immobilized by Pieters et al.[35] onto magnetic particles for maltodextrin hydrolysis thereby allowing for particle recovery with an electromagnet.

Backer et al.[36] developed a method whereby gel-immobilized cell systems can be analyzed for the effects of diffusional limitations and heterogeneous cell distribution. The system (see Figure 24) is a gel membrane bioreactor and simulates reaction and diffusion in a gel bead. The top of the gel equates to the outside of a gel bead while the bottom of the gel simulates the inner gel bead. Sampling chambers at the top and bottom (outer and inner) of the gel permit liquid and gas analysis. In this way the gel membrane bioreactor can be used for the study of diffusion and cellular reaction in a gel-immobilized cell system, which can subsequently lead to a mathematical model for substrate and cell concentrations in the gel matrix.

Table 7. Microcarrier characteristics.[a]

	R1[b]	R2	R3	R4
Specific gravity	2.21	2.36	2.27	2.65
Dry bulk density (g/mL)	0.44	0.31	0.46	1.53
Surface area (mi/g)	46	1.3	0.2	0.004
Pore volume (mi/g)	1.19	1.47	0.66	—
Volume fraction (mi/g)				
0.04–0.1 μm	0.23	0.01	—	—
0.1–1.0 μm	0.29	0.04	0.02	—
1.0–10.0 μm	0.28	0.88	0.10	—
10.0–50.0 μm	0.12	0.54	0.47	—
Mean pore diameter (μm)	0.14	6.5	30.9	—

a. Microcarrier size: 425–610 μm.

b. R1: Calcined diatomaceous earth and clay.
R2: Flux calcined diatomaceous earth.
R3: Calcined diatomaceous earth and clay.
R4: Ottawa silica sand.

Table 8. Average pseudo-steady-state reactor performance at an organic loading of 6 g. TOC/ l/day.

	R1	R2	R3	R4
HRT (h)	20	20	20	20
Feed TOC (mg/L)	5,000	5,000	5,000	5,000
Effluent TOC (mg/L)	50	40	40	150
Percent TOC removal	99	99	99	97
Immobilized cell				
Concentration (g/L)	15.4	40.0	20.7	5.0
Mass (g)	6.7	17.4	9.0	2.2
Percent of total cell mass	91	99	98	80
Free cell				
Concentration (mg/L)	338	147	92	278
Mass (g)	0.68	0.29	0.18	0.56
Percent of total cell mass	9	1	2	20

Table 8. (continued).

	R1	R2	R3	R4
Methane production				
Yield (l CH/g TOC)	1.01	0.95	1.05	0.97
Percent of biogas	65	70	65	70
MCRT (days)	38	226	188	15
Observed cell detachment rate (g VSS/g TOC)	0.055	0.026	0.025	0.064

R1: Calcined diatomaceous earth and clay.
R2: Flux calcined diatomaceous earth.
R3: Calcined diatomaceous earth and clay.
R4: Ottawa silica sand.

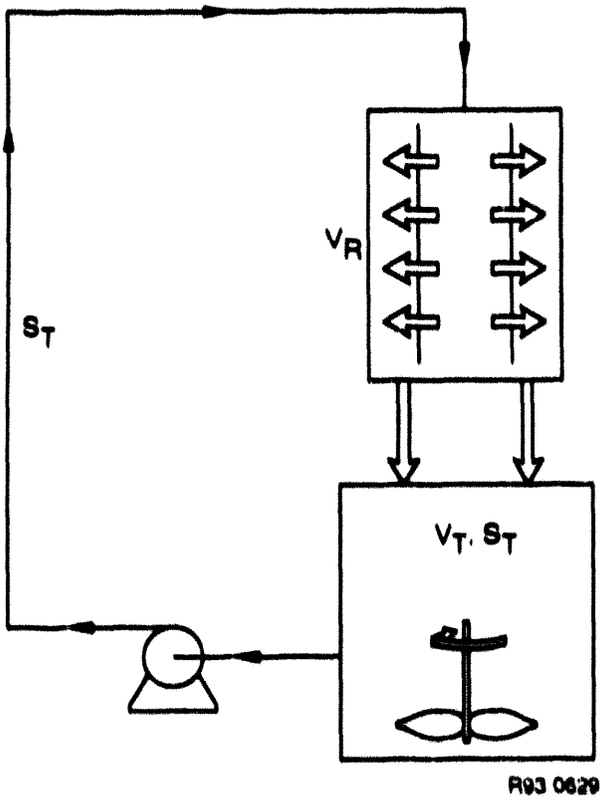

Figure 23. Ceramic microfilter reactor in dead-end configuration under batch-recycle operation.

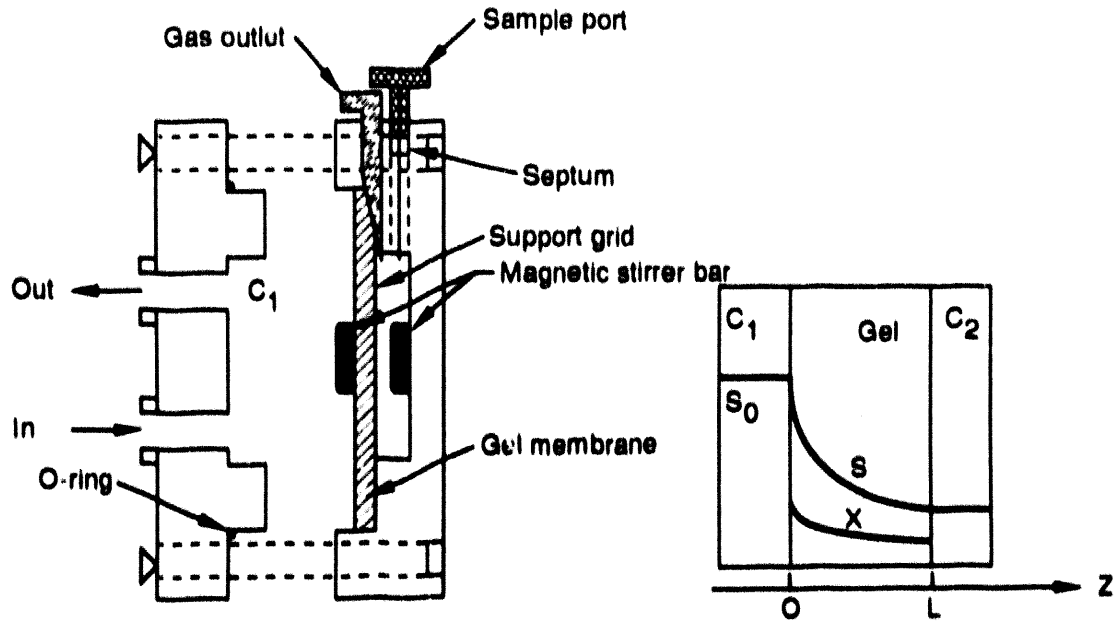

C_1 – First stirred chamber (open)

C_2 – Second stirred chamber (closed)

S – Substrate concentrations

S_o – Substrate concentration in chamber C_1

X – Immobilized biomass concentrations

O – Time = 0

L – Membrane thickness

Z – Time > 0

L93 0601

Figure 24. The gel membrane reactor.

PHOTOBIOREACTORS

Removal of carbon dioxide from industrial sources has been accomplished with the use of photosynthetic microorganisms. Although carbon dioxide is highly water soluble and poses little problem in mass transfer, the limiting factor in these systems is often light penetration through the bioreactor. Lee and Low[37] operated a bioreactor tilted at an angle facing the sun to increase solar radiation to the bioreactor and increase biomass yields relative to controls (see Figure 25). Results demonstrated that a photobioreactor operated at 80-degrees had a daily biomass output six times that of similar bioreactors operated in a horizontal position. Enhanced light penetration into a photobioreactor was accomplished with optical fibers.[38] Light energy distribution was accomplished by passing light through a bundle of optical fibers inside a column-type bioreactor (see Figure 26). The light was in the visible region of the spectrum (380–700 nm) with little infrared and reduced UV, from a 400 W metal halide lamp. This light diffusing optical fiber photobioreactor demonstrated potential for CO_2 removal and biomass production using marine algae.

Famiglietti et al.[39] contained the blue-green algae (*Anabaena variabilis*) in water-in-oil microemulsions containing (Tween85/Span80)/hexadecane/water. The result was a homogeneous microbial solution (cell density - 10^8 cells/mL) with photosynthetic activity taking place inside the emulsions because of their transparent nature. The emulsions also significantly prevented sedimentation of the cells when compared to unemulsified controls (see Figure 27).

Khan et al.[40] have demonstrated enhanced rates of hydrogen production compared to that of solar photovoltaic hydrogen systems by incorporating a biophotoelectrochemical system. This system uses bacteriorhodopsin in the purple membranes of *Halobacterium halobium* MMT_{22}, which is a light driven proton pump. *H. halobium* also produces hydrogen. The biophotoelectrochemical system (see Figure 28) consists of two chambers filled with a NaCl electrolyte solution and separated by a sintered glass disc. *H. halobium* MMT^{22} is located in one chamber and supported by a dialysis sack. This chamber also contains a silver and a platinum electrode

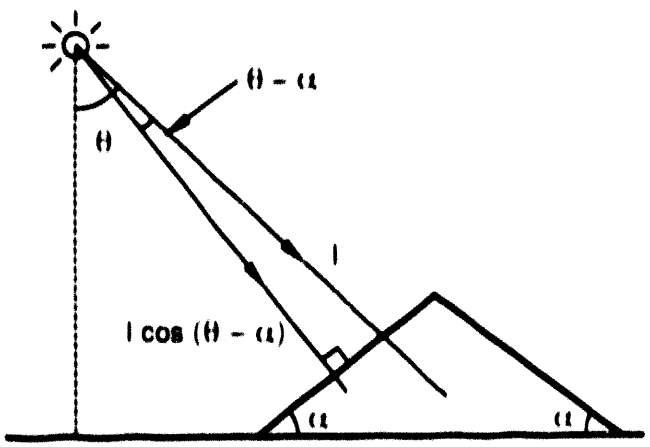

Figure 25. Bioreactor inclines at an angle with the horizontal.

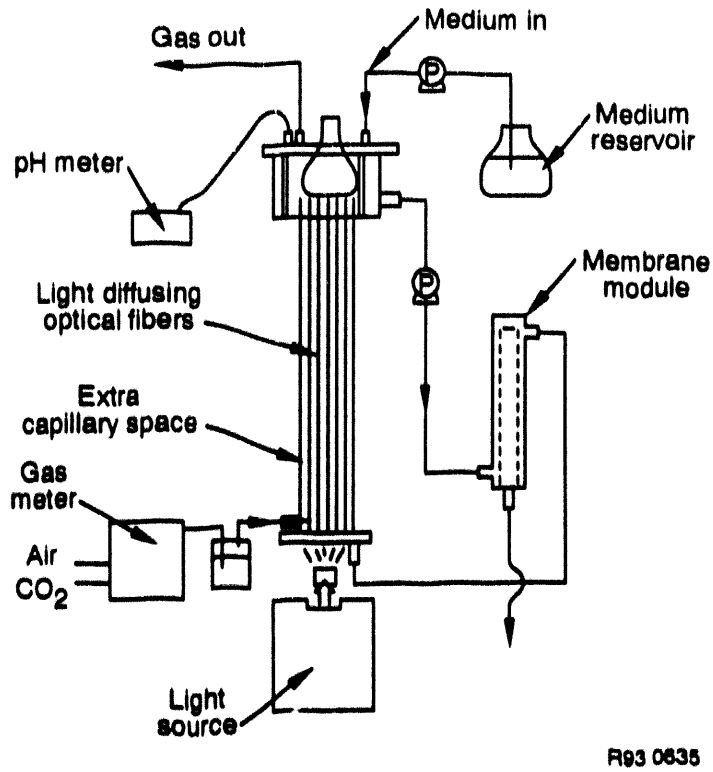

Figure 26. Schematic diagram of the light diffusing optical fiber photobioreactor system showing the ceramic membrane filtration module used for removing medium.

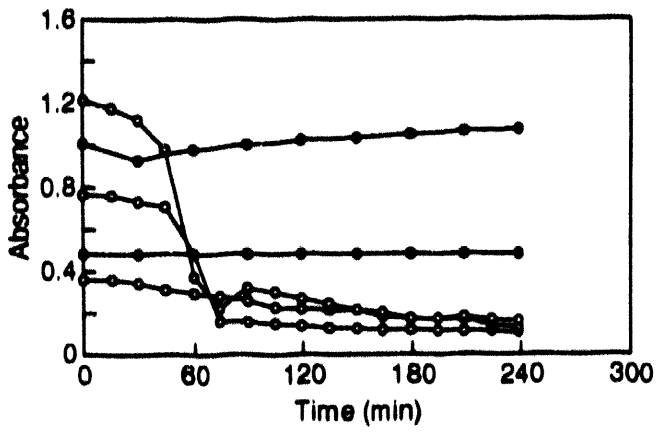

Figure 27. Sedimentation curves.

(see Figure 28). The other chamber contains one N/P silicone electrode with the P side insulated and the N side platinum coated. The external driving potential is applied between platinum electrodes kept outside the dialysis sack and the silicone electrode. Current is measured as it passes through the silicone cell. The solar insulation at the surface of the bacterium is also noted by using a solorimeter. Illumination of the system ultimately results in protons from *H. halobium* MMT_{22} and electrons from silicone combining and producing hydrogen.

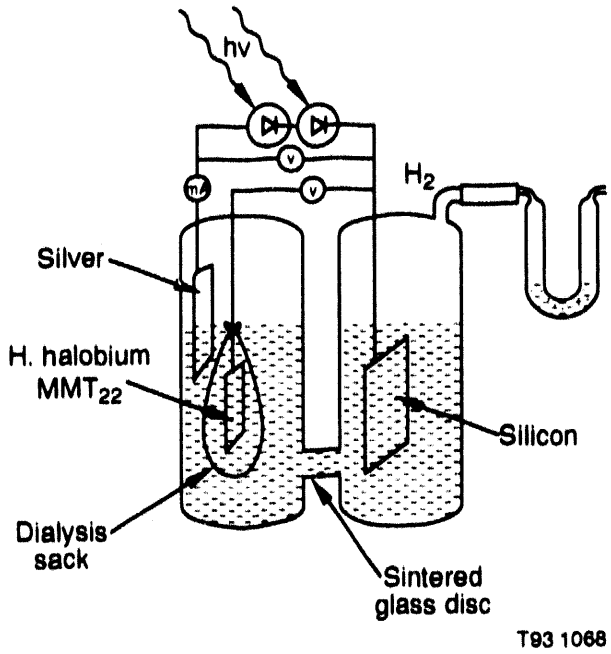

Figure 28. Schematic diagram of the apparatus used for solar hydrogen generation using *Halobacterium halobium* MMT_{22} and a silicon cell.

MICROBIAL INHIBITORS

Microbial activity can be negatively affected by inhibitory substances entering as part of the feedstock. This is especially common when treating a complex waste stream. Anaerobic treatment is quite prone to inhibition because of the sensitivity of parts of the microbial consortium, such as methanogens. Field et al.[41] demonstrated methanogenic inhibition during woody biomass fermentation. Cohen[42] surveyed several potential inhibitors to methanogenesis. Field et al.[41] added polyvinylpyrrolidone to liquid feedstocks before treatment to allow phenolics to bind with the polyvinylpyrrolidone and precipitate out.

Reduced performance in bioreactors can also be caused by metabolite inhibition. Buildup of microbial metabolites decreases bioreactor performance and often is caused by the inability to remove them from the bioreactor rapidly and economically. When these metabolites are of economic importance it is even more beneficial to remove them as rapidly as possible to minimize metabolite inhibition. This topic will be covered in the next section on by-product separation.

Several mathematical expressions were proposed by Thatipamala et al.[43] to describe the following:

1. Growth rate as a function of substrate inhibition:

$$\mu = \mu_m \left\{ \frac{S_{max} - S}{S_{max} - S_{min}} \right\} \qquad (24)$$

2. Instantaneous biomass yield as a function of product inhibition:

$$Y_{x/s} = \left(Y^0_{x/s} - Y^m_{x/s} \right) \left(\frac{1 - P}{P_m} \right)^n + Y^m_{x/s} \qquad (25)$$

3. Instantaneous biomass yield as a function of substrate inhibition:

$$Y_{x/s} = Y^0_{x/s} \left\{ \frac{S_{max} - S}{S_{max} - S_{min}} \right\} \qquad (26)$$

4. Lag time caused by substrate inhibition:

$$\frac{T_l}{(T_l)_{min}} = \left(\frac{S_o}{S_{min}} \right)^a \qquad (27)$$

where

S_{max} = maximum substrate concentration before inhibition is reached

S_{min} = minimum substrate concentration from where the growth rate (μ) is affected

$Y^0_{x/s}$ = maximum instantaneous biomass yield (dry weight)

$Y^m_{x/s}$ = minimum value of biomass approached by the overall biomass dry weight ($Y_{x/s}$) asymptotically as the product concentration P approaches the maximum (P_m)

n = power of product inhibition

T_l and $(T_l)_{min}$ = lag time and observed lag time at initial substrate concentration of the minimum substrate concentration (S_{min})

S_o = initial substrate concentration.

The removal of cresol from chemical mixtures containing nonphenolics was accomplished using a two-step process.[44] This process involved cresol as a model phenolic and its conversion to UV-absorbing by-products via tyrosinase, followed by chitosan absorption of only the by-products of cresol conversion. This method was specific for cresol removal and did not react with other chemicals present, which were anisol and benzyl alcohol (see Figure 29).

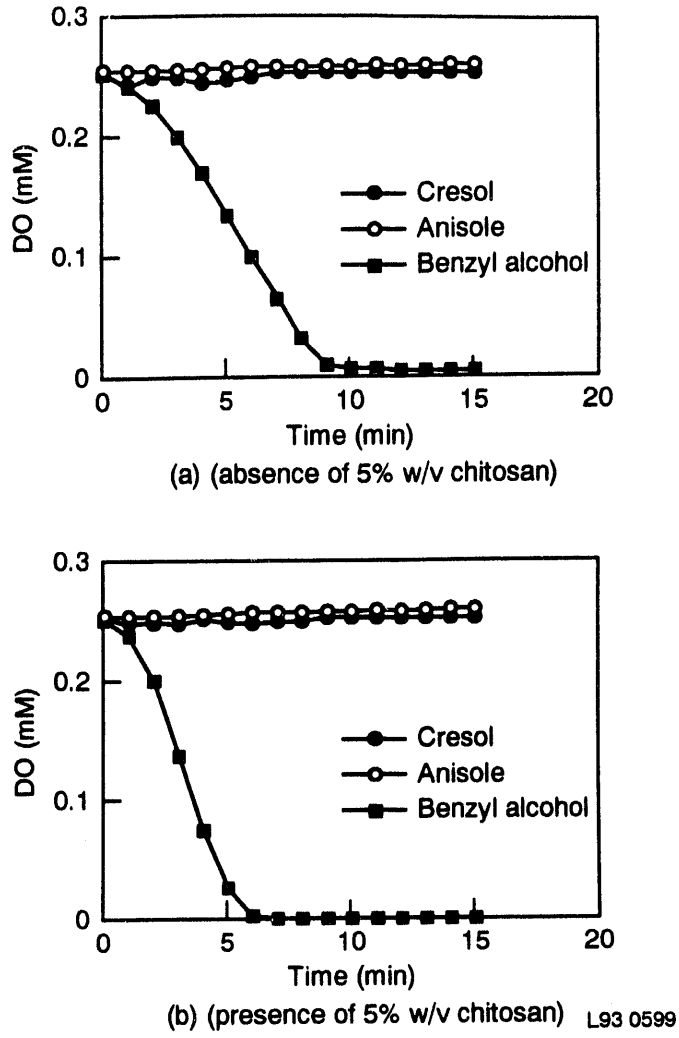

Figure 29. Selectivity of the tyrosinase-catalyzed reaction for phenols.

BY-PRODUCT SEPARATION

Desired by-products from a bioprocess can sometimes be separated easily because of their physical properties as gases or as precipitates. Other desired microbial metabolites remain in the liquid state and are difficult and expensive to remove. Many valuable chemical by-products need to be removed from bioreactors before they are transformed further to less valuable chemicals or initiate metabolite inhibition in the bioreactor. This problem reduces the cost-effectiveness of many bioprocesses. Removal of by-products from bioreactors has been accomplished in several ways (i.e., stripping, membrane solvent extraction, adsorption, pervaporation, electrodialysis, and liquid-liquid extraction).

Groot et al.[45] recovered butanol from a fluidized bed bioreactor incorporating five separate separation techniques (see Figures 30–35). Substrate is supplied with the feed and the bleed prevents accumulation of cells, by-products, and salts. Biocatalyst particles are fluidized in the bioreactor using a recirculation stream (see Figure 30). One method of product separation employed a closed loop column containing Raschig rings, a condenser, and a compressor. Butanol volatility was increased by setting the column temperature to 70°C, which also facilitated condensation of water and alcohol vapors (see Figure 31). Butanol removal from a fixed bed adsorber[45] was also accomplished by using polymeric resin XAD8 as the adsorbent. In spite of the low adsorption capacity of this material compared to active carbon, medium components did not foul the resin and therefore can be reused. Silicalite has a high selectivity and capacity for butanol adsorption,[46] but is prohibitive to use because of its high price.[45] Andrews and Fonta[47] analyzed ethanol production in a continuous, anaerobic bioreactor consisting of activated carbon, which facilitated ethanol removal in a circulating fluidized bed with about 10% of the ethanol produced (an inhibitory by-product) adsorbed to the carbon. Adsorption onto the activated carbon thereby decreases the ethanol concentration to the microbial biomass surrounding the activated carbon particle (see Figure 36). As biomass increases on the particle, inhibition is reduced and the particle moves to the bioreactor top, where it is removed for product recovery and then recycled back into the bioreactor.

Lactic acid removal from a biparticle fluidized bed bioreactor was possible because of the higher density of the sorbant particles (polyvinyl pyridine resin) compared to particles used to immobilize *Lactobacillus delbreuckii*[48] (see Figure 37). This fluidized bed bioreactor allowed the denser, adsorbent particles to fall further down in the column where they were removed for product recovery while the cells immobilized onto the less dense particles stayed in the bioreactor column. This nonoptimized configuration was capable of increasing the lactic acid yield by a factor of four.

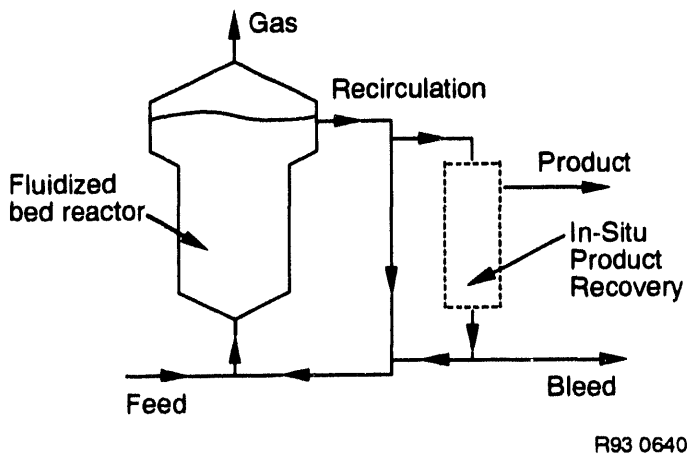

Figure 30. Integrated butanol production processes. Schematic of a fluidized bed reactor.

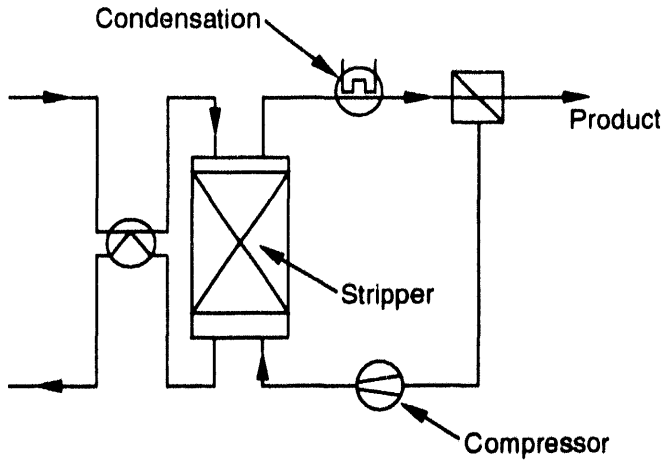

Figure 31. Schematic of a stripping process for in situ butanol recovery.

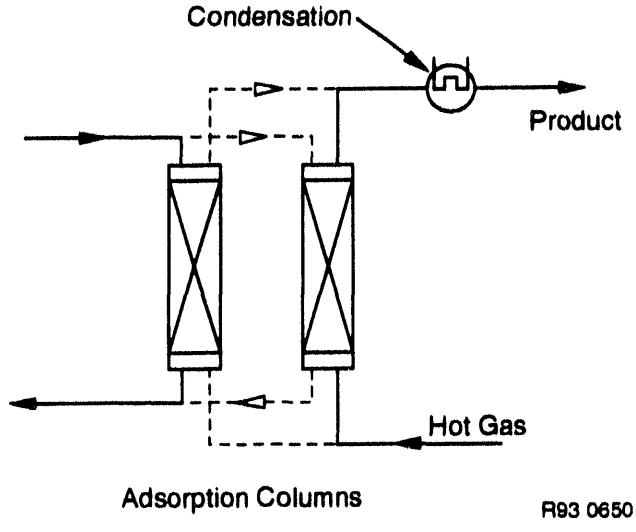

Figure 32. Schematic of an adsorption process for in situ butanol recovery.

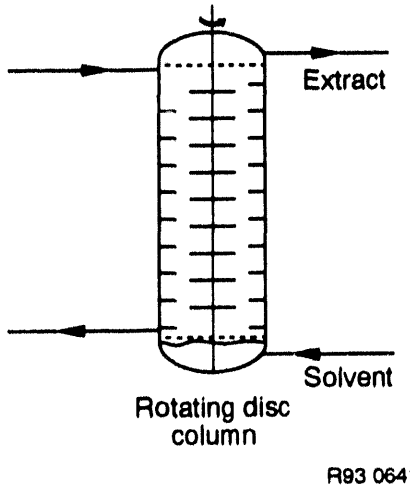

Figure 33. Schematic of a liquid-liquid extraction process for in situ butanol recovery.

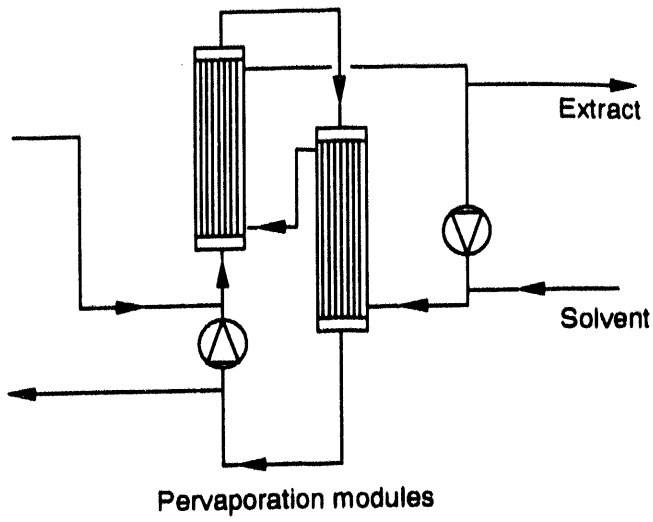

Figure 34. Schematic of a pervaporation process for in situ butanol recovery.

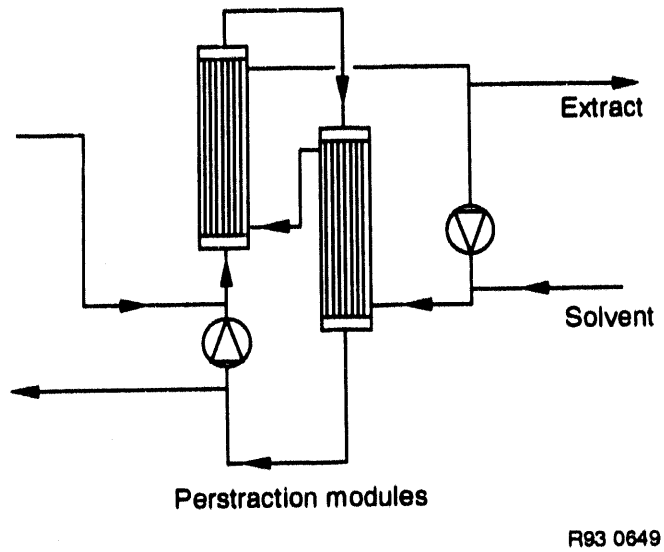

Figure 35. Schematic of a membrane solvent extraction process for in situ butanol recovery.

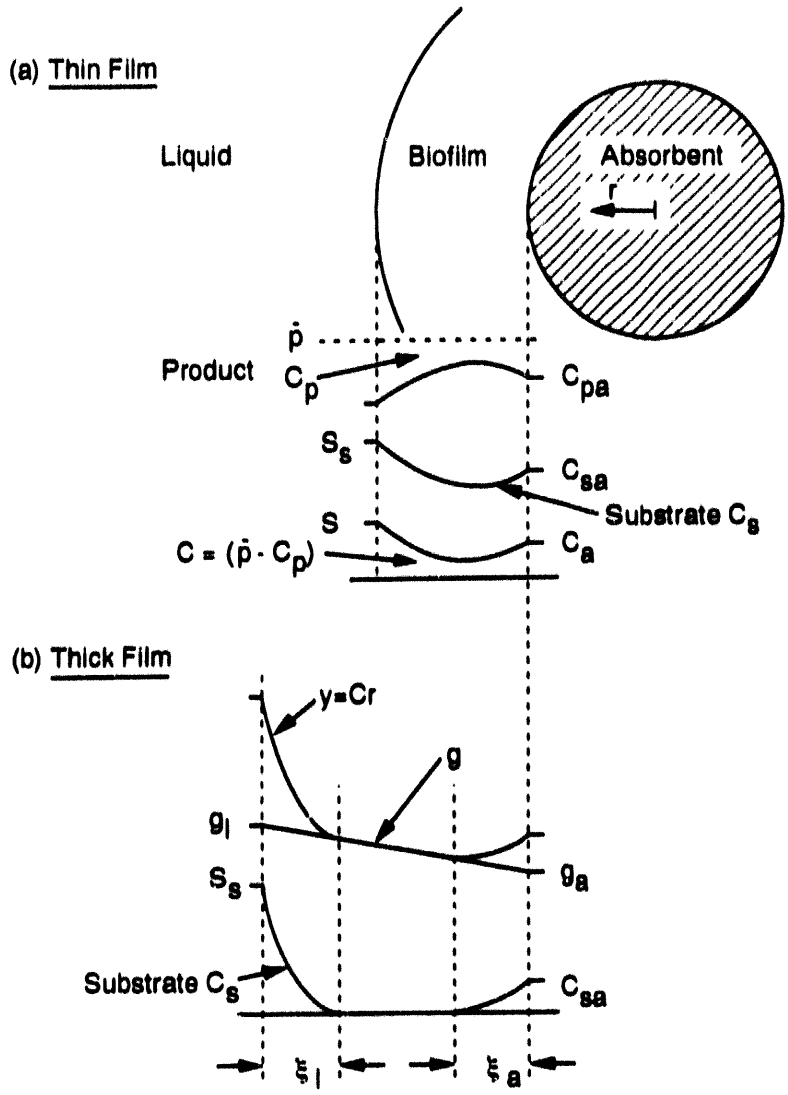

g – Related to what limits metabolic activity

(-) – Designates product inhibitors

(+) – Designates substrate exhaustion limits metabolic activity

ṗ – Completely inhibitory product concentration in liquid

r – Distance from particle center

S – Component concentrations in liquid

ξ – Active depth in a thick film

a – Value at absorbent side of film

c – Component concentrations in biomass

l – Value at Liquid side of film

p – Product

s – Substrate

L93 0598

Figure 36. Concentration profiles in the biofilm.

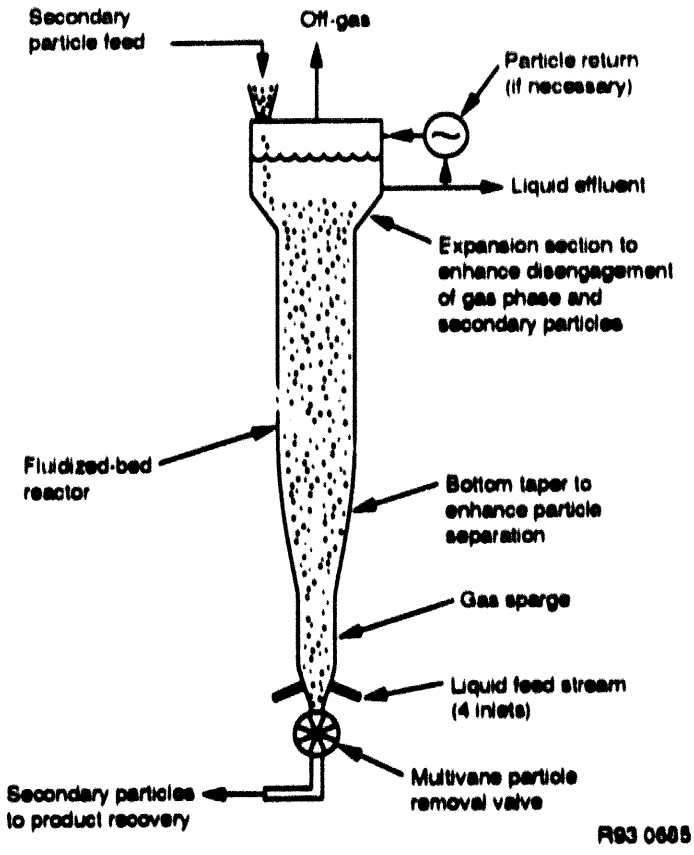

Figure 37. Schematic of experimental biparticle fluidized-bed bioreactor operating in the countercurrent mode.

Many authors have been successful in the physical recovery of desired compounds by using pervaporation techniques. This method employs semipermeable membranes that allow for the removal of microbial by-products but retains other liquid constituents of the growth medium. Masawaki et al.[49] separated the bioreactor feedstock butanol from a mixture of butanol-oleyl alcohol by using a poly(dimethylsiloxane) (PDMS) hollow fiber membrane (see Figure 38). This was accomplished at various temperatures, pressures, and butanol concentrations in the feed solution. The separation factor for butanol in the permeate [(Y_B (mole fraction)] increased with increasing temperature and feed butanol concentration [(X_B (mole fraction)] (see Figure 39).

In related work, the transport of phenol from an aqueous solution to butyl acetate was more efficient with a membrane of cross-linked poly(4-vinylpyridine) when compared to polyethylene, polypropylene, and polytetrafluoro-ethylene[50] (see Table 9). Shabtai et al.[51] demonstrated continuous ethanol production and separation by using an immobilized yeast in a continuous bioreactor coupled with a pervaporation membrane, consisting of a 2 μm polysiloxane composite on a polysulfone support (see Figure 40). The combined system consisted of two recirculation loops for the medium input and for ethanol exit from the bioreactor to the pervaporation unit. This operation yielded a continuous ethanol production (1,000 h) at a concentration of up to 20% (wt/vol).

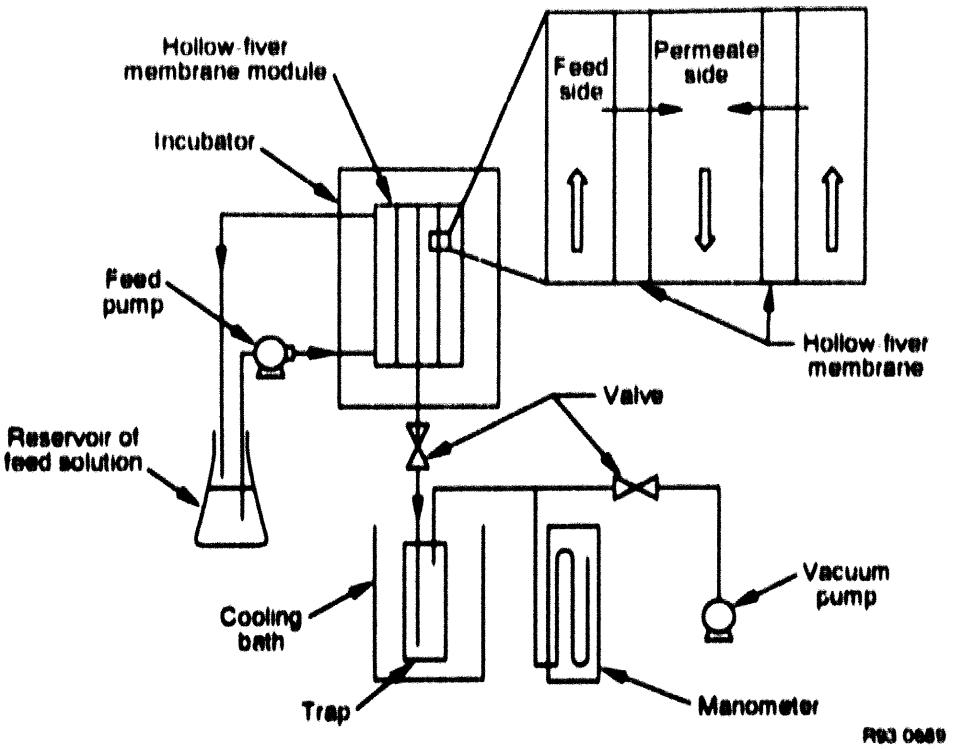

Figure 38. Schematic diagram of apparatus for pervaporation by hollow-fiber module.

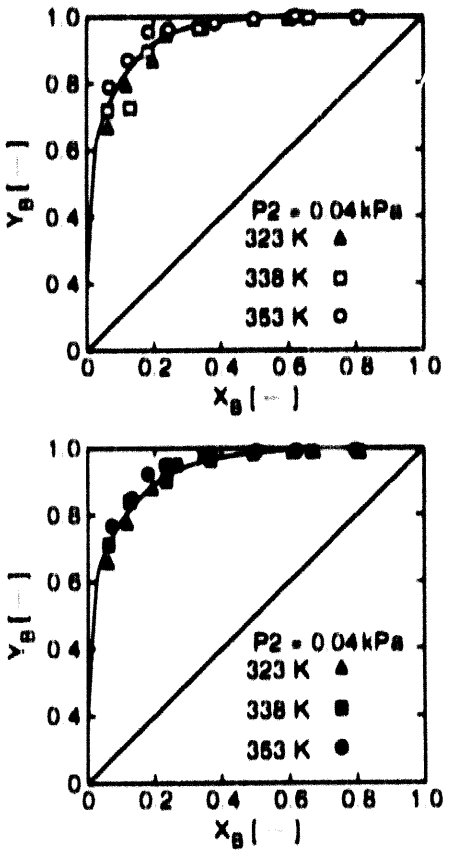

Figure 39. Relation between mole fraction of butanol in feed solution and that in permeate solution.

Table 9. Permeability of phenol through commercial membranes.

Membrane	Porosity	Pore diameter (μm)	Thickness (μm)	P (10^{-3} cm/sec)
PVP	0.50	0.08	200	2.22
PE	0.50	0.08	250	0.178
PP	0.38	0.02	25.3	1.02
PTFE	0.57	0.1	60	0.97

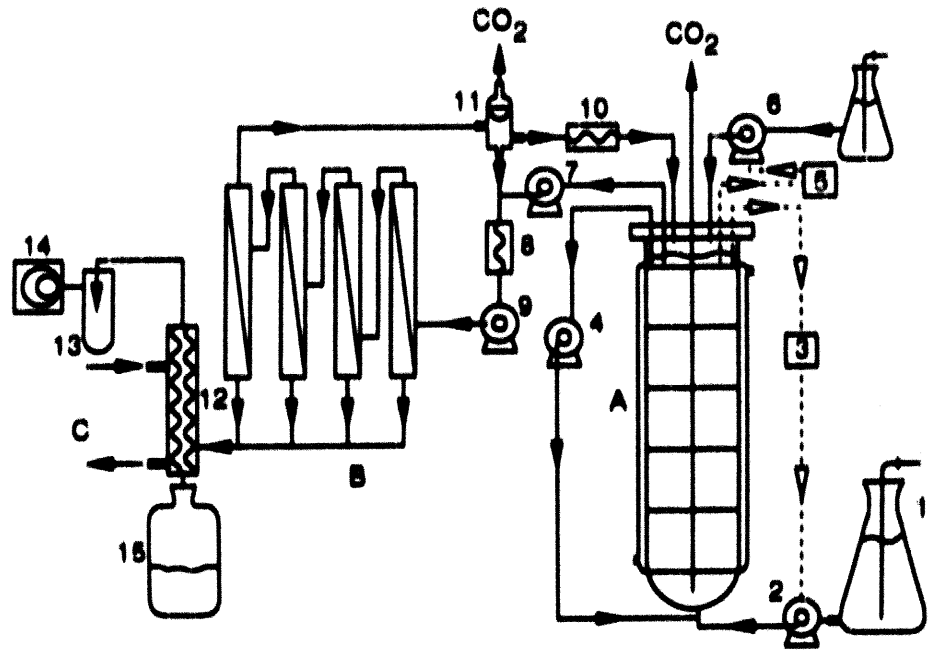

Schematic description of the coupled system

A = Immobilized yeast reactor
B = Membrane pervaporation unit
C = Product recovery unit

The concentrated sugar solution is fed from reservoir 1 by means of the peristaltic pump 2, which is actuated by a level controller 3. The medium inside the reactor is circulated by means of pump 4 (4.5 L/h) and its pH controlled by base addition through pump 6 using controller 5. Fermented medium is driven into the membrane pervaporation module (B) by means of pump 7. The temperature is adjusted to 45°C by the heat exchanger 8. The liquid is quickly circulated over the upstream side of the membrane (9 L/min) by pump 9 and returned gravitationally to the reactor after cooling to 30°C by the heat exchanger 10. A floating pressure relief device 11 installed in the outlet of the membrane circulating loop enabled this medium return by preventing pressure buildup and allowing the release of CO_2. The downstream side of the membrane is connected to the product recovery unit (C) consisting of a cooling coil 12, held at -19°C, a liquid nitrogen trap 13 and a vacuum pump14 maintaining the vacuum at 30 mb. The final concentrated pervaporate is collected in vessel 15.

L93 0596

Figure 40. Schematic description of the coupled system.

By-product removal using pervaporation, applied to acetone-butanol-ethanol (ABE) production in fluidized bed bioreactors may make this fermentation process economically viable relative to traditional technologies.[52] The bioreactor used *Clostridium acetobutylicum* immobilized onto bonechar with concentrated whey permeate, as the feedstock. Effluent from the bioreactor was cycled through the pervaporation chamber for by-product removal and then cycled back to the bioreactor (see Figure 41). Silicone tubing with a wall thickness of 0.4 mm was used as the membranes in a pervaporation chamber, located downstream of the bioreactor. Oxygen-free gas sweeping was used to remove ABE from the membrane surface. ABE were condensed at -3°C.

Groot et al.[45] examined five methods for butanol removal and determined that pervaporation and liquid-liquid extraction demonstrated greater potential than stripping, adsorption, or membrane solvent extraction. These findings are specific for one process but can be used to demonstrate feasibility of removal strategies for similar fermentation technologies.

Cho and Shuler[53] developed a multimembrane bioreactor incorporating pervaporation and membrane solvent extraction that consisted of immobilized yeast sandwiched between a hydrophobic membrane above and a hydrophilic membrane below (see Figure 42). The hydrophobic membrane allowed for oxygen transport to the cells and CO_2 removal from the system. While the nutrient solution entered the cell layer through the hydrophilic membrane, ethanol exited the cell layer through the same membrane, traveled through the nutrient solution stream and through another hydrophobic membrane into a solvent solution stream for product recovery. This process required no external energy but was driven by the free energy of the system.

Electrodialysis has been shown to be effective in the removal of L-lactate,[54,55,56,57,58] acetic acid,[59,60] and L-lysine[58] from batch fermenters. This process involves the removal of the dissociated end product from solution using electrodialysis. This has been demonstrated to reduce end product inhibition in batch fermentations. The electrodialysis system consisted of platinum plates that served as anode and cathode with a current of 0.2–0.6 amperes. During electrodialysis, the fermentation broth (pH regulated at 6.0 with 2N NaOH) and anolyte (0.1N H_2SO_4) were circulated through the system where the end product was continuously extracted by the electrodialyzer and maintained at levels that decreased end product inhibition. One drawback is that cells contacting the dialysis membrane were killed. This was avoided by installing a microfiltration module upstream of the electrodialyzer[57] (see Figure 43).

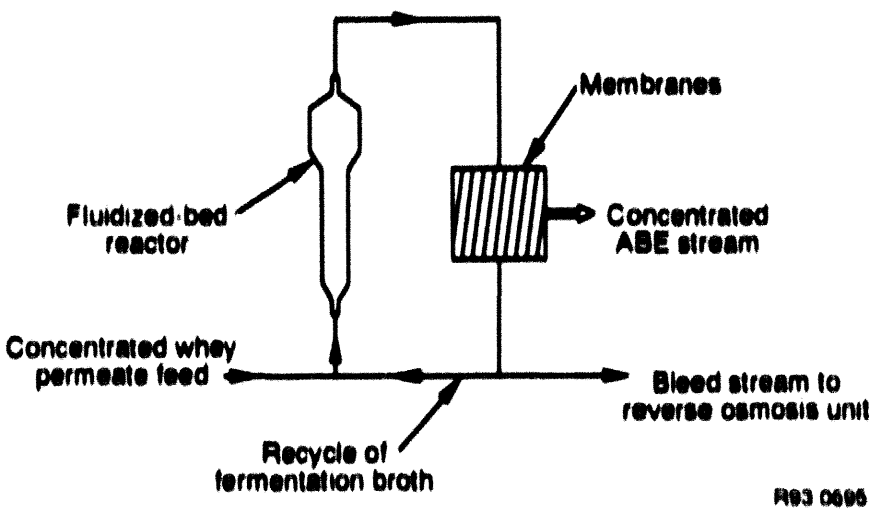

Figure 41. Schematic diagram of integrated continuous fermentation/product removal for ABE production.

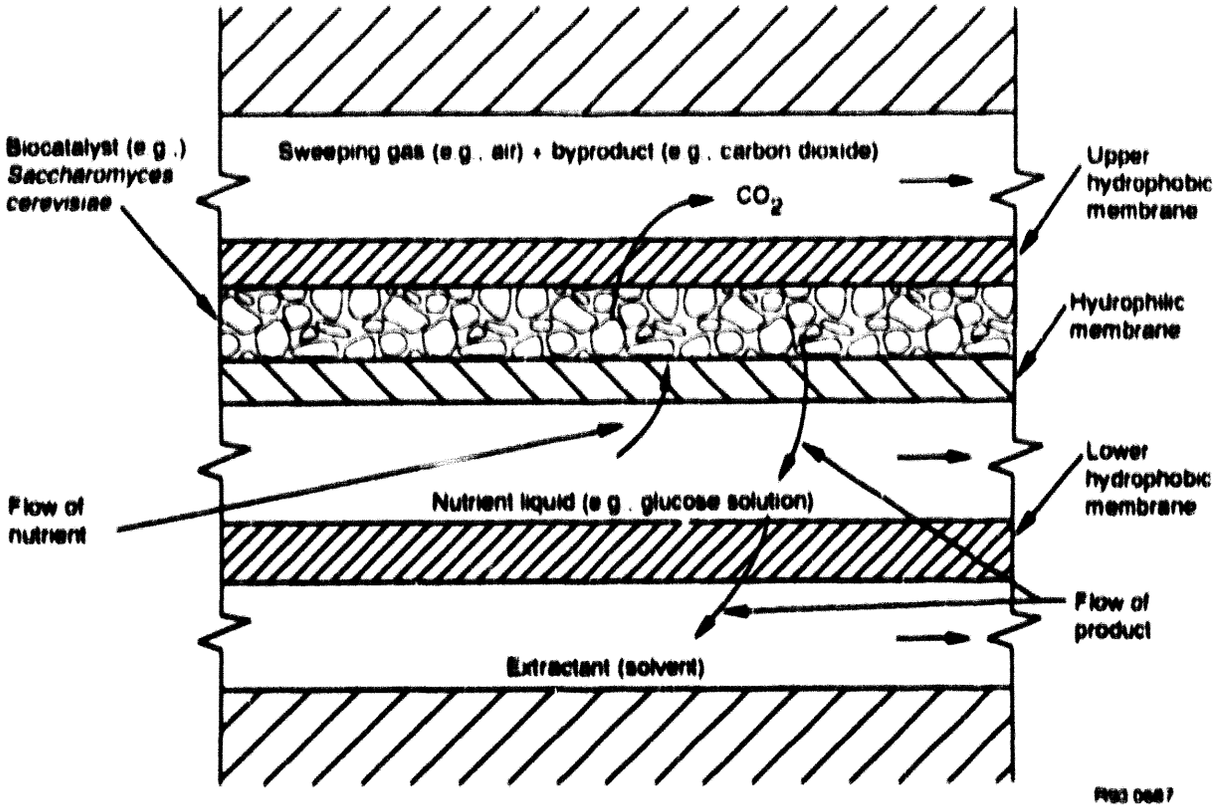

Figure 42. Example of multilayer membrane bioreactor.

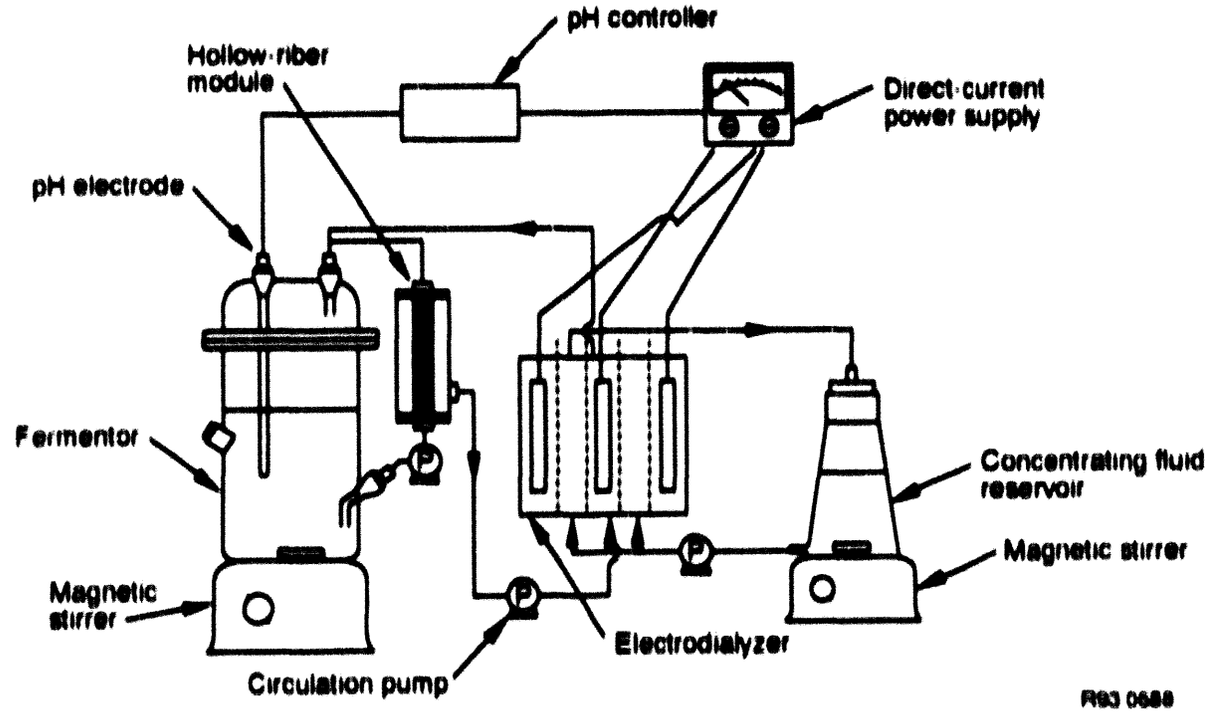

Figure 43. Schematic diagram of system for ED-F with an MF module.

ELECTROCHEMICAL AND ELECTROLYTIC BIOREACTORS

Miyawaki and Yano[61] defined an electrochemical bioreactor as a "reactor in which an oxidoreductase reaction is conjugated with an electrochemical reaction at the electrode." The bioreactor constructed by Miyawaki and Yano[61] consisted of a rotating graphite rod and disc onto which phenazine methosulfate (PMS) was adsorbed. The rod and disc were operated inside 200 mL of a 0.1M phosphate buffer with oxygen removed by bubbling high purity nitrogen gas through the liquid. The bioreactor was connected to a conventional three electrode system controlled by a potentiastat. Cyclic voltammetry measurements were used to determine the electrochemical oxidation of NADH (see Figure 44) and were obtained using a function generator to produce a potential sweep signal. This bioreactor allowed for the regeneration of NAD^+ to NADH by using the enzyme system G6PDH with adsorbed PMS (see Figure 45) to act as a mediator reducing the tendency of high overpotential in NAD^+ regeneration for the reactions in Figure 46. This bioreactor design has potential for use with immobilized enzymes for biosensors, biohydrometallurgy, and biochemical transformations.

Yunker and Radovich[62] developed an electrolytic fermentation process for enhancing the growth and increasing cell density of *Thiobacillus ferrooxidans* by regenerating ferrous ions used by the cell as an energy source. The ferrous ions are regenerated by reducing the ferric ions at the cathode by passing a current through the fermentation medium. This method increased bacterial density in the bioreactor by minimizing the inhibitory effects on cell growth by ferric ions as well as minimizing limitations caused by substrate depletion. Current from 250–1,000 ma through the bioreactor resulted in increased growth and cell density as measured by cell protein. Electrolyzed cells also demonstrated a shorter generation time compared to control cells. Techniques such as this can assist in obtaining high cell densities of organisms where other methods have proved inadequate.

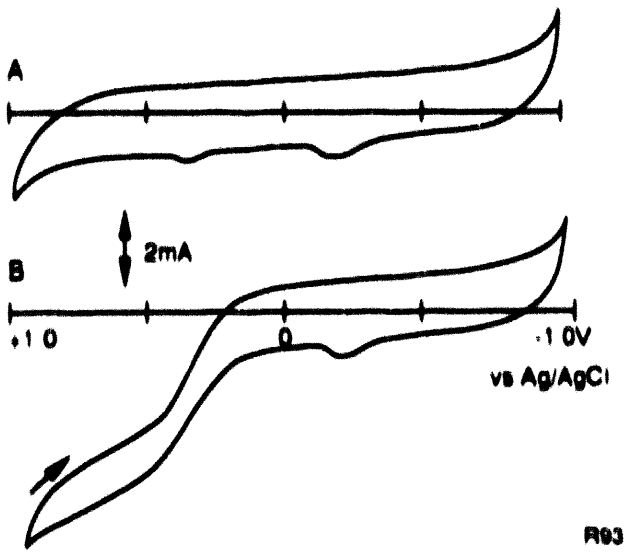

Figure 44. Cyclic voltammogram of electrochemical oxidation of NADH in an electrochemical bioreactor.

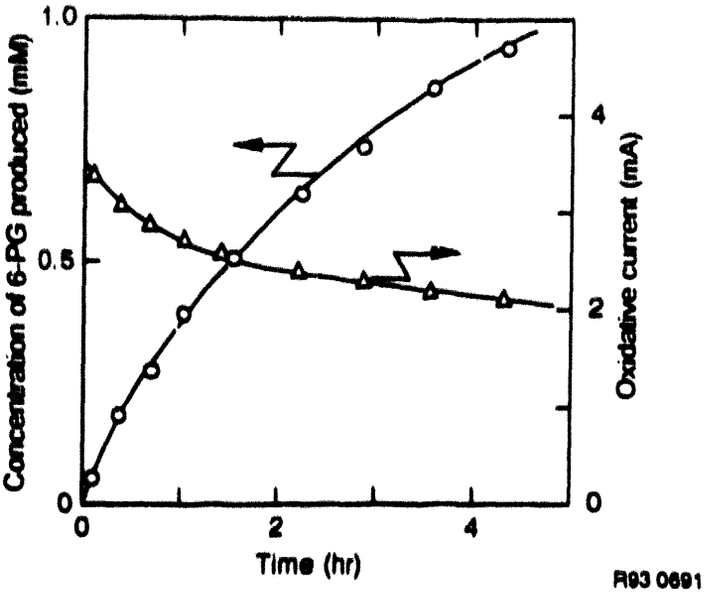

Figure 45. G6PDH reaction conjugated with constant potential.

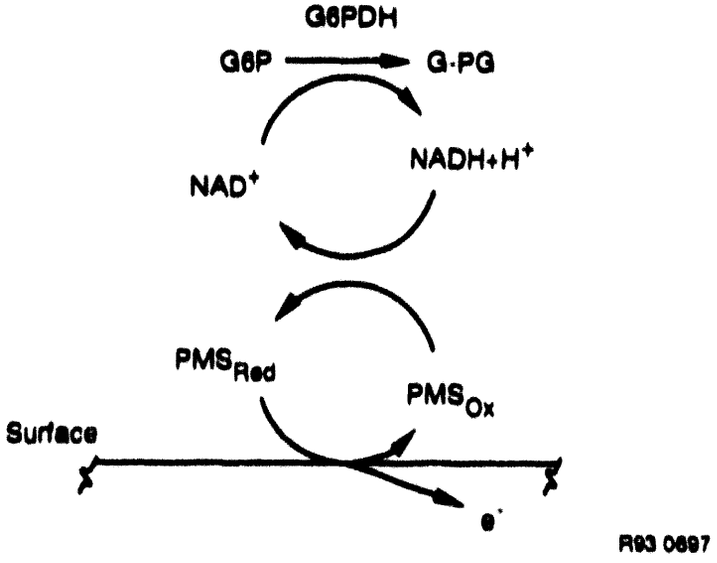

Figure 46. NAD regeneration system by G6PDH in an electrochemical bioreactor.

FUTURE AREAS OF STUDY

Bioreactor designs and bioprocessing strategies reported here should provide a bases for continued developments and improvements of bioprocesses in future work. Specific areas of research that may provide the most potential in improving the economic potential of biotechnology include advanced by-product separation procedures, simplified bioreactor designs capable of economically increasing gas and liquid mass transfer, improved cell and enzyme immobilization techniques, and electrochemical bioprocesses.

The economic potential of individual bioprocesses will also increase if they are designed to serve multiple purposes such as bioremediation and by-product production. An example would be methane bioconversion to methanol, single cell protein or both, all incorporated in one bioprocess. In this way the cost of a bioprocess designed for bioremediation could be offset by the simultaneous bioconversion of a particular waste to a marketable product.

REFERENCES

1. K. T. Klasson, M. D. Ackerson, E. C. Clausen, and J. L. Gaddy, "Mass-Transport in Bioreactors for Coal Synthesis Gas Fermentation," *Fuel, V204*, 1992, p.125.

2. K. T. Klasson, M. D. Ackerson, E. C. Clausen, and J. L. Gaddy, "Biological Conversion of Synthesis Gas Into Fuels," *International Journal of Hydrogen Energy, V17*, N4, 1992, pp. 281–288.

3. H. Brauer, "Growth of Fungi and Bacteria in the Reciprocating Jet Bioreactor," *Bioprocess Engineering, 6*, 1991, pp. 1–15.

4. H. Brauer and A. P. Annachhatre, "Waste-Water Nitrification Kinetics Using Reciprocating Jet Bioreactor," *Bioprocess Engineering, V7*, N6 (MAR), 1992, pp. 277–286.

5. W. Grueger and H. Brauer, Verfahrenstechnische Untersuchung der Abwasserreinigung im Hubstrahlreaktor. VDI-Forschungsheft 643. VDI-Verlag GmbH, Düsseldorf, 1987.

6. Y. Shi, D. D. Y. Ryu, and S. H. Park, "Performance of Mammalian Cell Culture Bioreactor with a New Impeller Design," *Biotechnology and Bioengineering, 40*, 1992, pp. 260–270.

7. M. Reiter, F. Weigang, W. Ernst, and H. W. D. Katinger, "High Density Microcarrier Culture with a New Device which allows Oxygenation and Perfusion of Microcarrier Cultures," *Cytotechnology, 3*, 1990, pp. 39–42.

8. T. Ahmed and M. J. Semmens, "Use of Sealed End Hollow Fibers for Bubbleless Membrane Aeration: Experimental Studies," *Journal of Membrane Science, 69*, 1992, pp. 1–10.

9. O. Hirasa, H. Ichijo, and A. Yamauchi, "Oxygen Transfer from Silicone Hollow Fiber Membrane to Water," *Journal of Fermentation and Bioengineering, 71*, 1991, pp. 206–207.

10. S. Beeton, H. R. Millward, B. J. Bellhouse, A. M. Nicholson, N. Jenkins, and C. J. Knowles, "Gas Transfer Characteristics of a Novel Membrane Bioreactor, *Biotechnology and Bioengineering, V38*, N10, 1991, pp. 1,233–1,238.

11. W. T. Wu, J. Y. Wu, and J. Z. Jong, "Mass Transfer in an Airlift Reactor with a Net Draft Tube," *Biotechnology Progress, 8*, 1992, pp. 465–468.

12. H. S. Jee, N. Nishio, and S. Nagai, "CH_4 Production from H_2 and CO_2 by *Methanobacterium thermoautotrophicum* Cells Fixed on Hollow Fibers," *Biotechnology Letters, 10*, 1988, pp. 243–248.

13. T. Yano, K. Aoki, and S. Nagai, "Kinetics of CH_4 Production from H_2 and CO_2 in a Hollow Fiber Reactor by Plug Flow Reaction Model," *Journal of Fermentation and Bioengineering, 71*, 1991, pp. 203–205.

14. W. A. Apel, P. R. Dugan, and M. R. Wiebe, "Influence of Kaolin on Methane Oxidation by *Methylomonas methanica* in Gas Phase Bioreactors," *Fuel, 71*, 1992, pp. 805–808.

15. W. A. Apel, P. R. Dugan, and M. R. Wiebe, "Use of Methanotrophic Bacteria in Gas Phase Bioreactors to Abate Methane in Coal Mine Atmospheres," *Fuel, 70*, 1991, pp. 1,001–1,003.

16. M. A. Applegate and G. Stephanopoulos, "Development of a Single-Pass Ceramic Matrix Bioreactor for Large-Scale Mammalian Cell Culture," *Biotechnology and Bioengineering, 40*, 1992, pp. 1,056–1,068.

17. C. M. Nelson, M. R. Schuppenhauer, and D. S. Clark, "High-Pressure, High-Temperature Bioreactor for Comparing Effects of Hyperbaric and Hydrostatic Pressure on Bacterial Growth," *Applied and Environmental Microbiology, 58*, 1992, pp. 1,789–1,793.

18. M. Torrijos, *Evaluation des techniques non conventionnelles d'intensification des transfers d'oxygène en fermentation*, Thèse Docteur Ingénier I.N.S.A., Toulouse, France, 1987.

19. P. Adlercreutz and B. Mattiasson, "Oxygen Supply to Immobilized Cells," *European Journal of Applied Microbiology and Biotechnology, 16*, 1982, pp. 165–170.

20. C. Khosla and J. Bailey, *Technical Support Package on: More Genetic Engineering with Cloned Hemoglobin Genes," NASA Tech Brief Vol. 16, No. 11, Item #94 from JPL New Technology Report NPO-18156-7669*, 1992.

21. J. L. Rols and G. GOMA, "Enhancement of Oxygen-Transfer Rates in Fermentation Using Oxygen-Vectors," *Biotechnology Advances, V7*, 1989, pp. 1–14.

22. A. T. King, B. J. Mulligan, and K. C. Lowe, "Perfluorochemicals and Cell Culture," *Biotechnology, 7*, 1989, pp. 1,037–1,042.

23. D. Damiano and S. S. Wang, "Novel Use of a Perfluorocarbon for Supplying Oxygen to Aerobic Submerged Cultures," *Biotechnology Letters, 7*, 1985, pp. 81–86.

24. L. K. Ju, J. F. Lee, and W. B. Armiger, "Enhancing Oxygen-Transfer in Bioreactors by Perfluorocarbon Emulsions," *Biotechnology Progress, V7*, N4, 1991, pp. 323–329.

25. Ceschin, C., M.C. Malet-Martino, G. Michel and A. Lattes. 1985. C.R. Acad. Sc. Paris, Ser.III 18, pp. 669–672.

26. R. H. Douglass, J. M. Armstrong, and W.M. Korreck Design of a Packed Column Bioreactor for on-Site Treatment of Air Stripper Off Gas On-Site Bioreclamation (1991) pp. 209–225, eds. R. F. Hinchee and R. F. Olfenbuttel, Publisher Butterwood-Heinemann.

27. T. O. Williams and F. C. Miller, "Biofilters and Facility Operations," *BioCycle*, 1992, pp. 75–79.

28. R. S. Tiwaree, K. S. Cho, M. Hirai, and M. Shoda, "Biological Deodorization of Dimethyl Sulfide Using Different Fabrics as the Carriers of Microorganisms," *Applied Biochemistry and Biotechnology, 32*, 1992, pp. 135–148.

29. S. K. Lee and M. Shoda, "Biological Deoderization Using Activated Carbon Fabric as a Carrier of Microorganisms," *Journal of Fermentation and Bioengineering, 68*, 437, 1989.

30. G. E. Speitel and J. M. Leonard, "A Sequencing Biofilm Reactor for the Treatment of Chlorinated Solvents Using Methanotrophs," *Water Environment Research, 64*, 1992, pp. 712–719.

31. V. P. Lewis and S. T. Yang, "Continuous Propionic Acid Fermentation by Immobilized *Propionibacterium acidipropionici* in a Novel Packed-Bed Bioreactor," *Biotechnology and Bioengineering, 40*, 1992, pp. 465–474.

32. N. Nishio, E. Kayawake, and S. Nagai, "Rapid Methane Production from Formate or Acetate in Fixed Bed Bioreactors," *Journal of Fermentation Technology, 63*, 1985, pp. 205–209.

33. C. J. Yee, Y. Hsu, and W. K. Shieh, "Effects of Microcarrier Pore Characteristics on Methanogenic Fluidized Bed Performance," *Water Research 26*, 1992, pp. 1,119–1,125.

34. T. J. Harrington, J. L. Gainer, and D. J. Kirwan, "Ceramic Membrane Microfilter as an Immobilized Enzyme Reactor," *Enzyme Microbial Technology, 14*, 1992, pp. 813–818.

35. B. R. Pieters, G. Bardeletti, and P. R. Coulet, "Glucoamylase Immobilization on a Magnetic Microparticle for the Continuous Hydrolysis of Maltodextrin in a Fluidized Bed Reactor," *Applied Biochemistry and Biotechnology, 32*, 1992, pp. 37–53.

36. L. Backer, S. Devleminck, R. Willaert, and G. Baron, "Reaction and Diffusion in a Gel Membrane Reactor Containing Immobilized Cells," *Biotechnology and Bioengineering, 40*, 1992, pp. 322–328.

37. Y. K. Lee and C. S. Low, "Effect of Photobioreactor Inclination on the Biomass Productivity of an Outdoor Algal Culture," *Biotechnology and Bioengineering, 38*, 1991, pp. 995–1,000.

38. H. Takano, H. Takeyama, N. Nakamura, K. Sode, J. G. Burgess, E. Manabe, M. Hirano, and T. Matsunaga, "CO_2 Removal by High-Density Culture of a Marine Cyanobacterium Synechococcus sp. Using an Improved Photobioreactor Employing Light-Diffusing Optical Fibers," *Applied Biochemistry and Biotechnology 34*, 1992, pp. 449–458.

39. M. Famiglietti, A. Hochkoppler, E. Wehrli, and P. L. Luisi, "Photosynthetic Activity of Cyanobacteria in Water-in-Oil Microemulsions," *Biotechnology and Bioengineering, 40*, 1992, pp. 173–178.

40. M. M. T. Kahn, M. R. Adiga, and J. P. Bhatt, "Large Scale Photobiological Solar Hydrogen Generation Using Halobacterium Halobium MMT_{22} and Silicon Cell," *Journal of Hydrogen Energy*, 17, 1992, pp. 93–95.

41. J. A. Field, M. J. H. Leyendeckers, R. Sierra-Alvarez, G. Lettinga, and L. A. A. Habets, "The Methanogenic Toxicity of Bark Tannins and the Anaerobic Biodegradability of Water Soluble Bark Matter," *Water Science and Technology, 20*, 1, 1988, pp. 219–240.

42. A. Cohen, "Effects of Some Industrial Chemicals on Anaerobic Activity Measured by Sequential Automated Methanometry (SAM)," *Water Science and Technology, 25*, 1992, pp. 11–20.

43. R. Thatipamala, S. Rohani, and G. A. Hill, "Effects of High Product and Substrate Inhibitions on the Kinetics and Biomass and Product Yields during Ethanol Batch Fermentation," *Biotechnology and Bioengineering, 40*, 1992, pp. 289–297.

44. G. F. Payne, W. Q. Sun, and A. Sohrabi, "Tyrosinase Reaction/Chitosan Adsorption for Selectively Removing Phenols from Aqueous Mixtures," *Biotechnology and Bioengineering, 40*, 1992, pp. 1,011–1,018.

45. J. W. Groot, R.G. J. M. Vanderlans, and K. C. A. M. Luyben, "Technologies for Butanol Recovery Integrated with Fermentations," *Process Biochemistry 27*, 2, 1992, pp. 61–75.

46. N. B. Milestone and D. M. Bibby, *Journal of Chemical Technology and Biotechnology, 31*, 1981, p. 1.

47. G. F. Andrews and J. P. Fonta, "A Novel Adsorbing Bioreactor," *Biotechnology and Bioengineering Symposium, No. 17*, 1986, pp. 317–333.

END

DATE FILMED

12/23/93